NOZZLE/COWL OPTIMIZATION FOR A HYPERSONIC VEHICLE ON A TYPICAL TRAJECTORY

THESIS

Michael J. Bonaparte

AFIT/GAE/ENY/92D-10

AFIT/GAE/ENY/92D-10

NOZZLE/COWL OPTIMIZATION FOR A HYPERSONIC VEHICLE ON A TYPICAL TRAJECTORY

THESIS

Presented to the Faculty of the School of Engineering

of the Air Force Institute of Technology

Air University

In Partial Fulfillment of the

Requirements for the Degree of

Master of Science in Aeronautical Engineering

Michael J. Bonaparte

December 1992

Approved for public release; distribution unlimited

Acknowledgements

I want to thank Captain John Doty for his patience and guidance as I undertook this research. His thought provoking comments and assistance helped me to organized and present the ideas and results of this work.

I also want to thank my children, Michelle, Maria, and Denise, for giving me the time necessary to complete this task. Finally, I want to express my deepest gratitude to my wife, Yvonne, for her never ending support of my efforts. With her positive attitude of my abilities and her encouragement to carry me forth, this task is now completed in her honor.

Table of Contents

List of Figures

List of Tables

List of Symbols

a	speed of sound
a	first coefficient in quadratic curve equation
a	first coefficient in equation for specific heat at constant pressure
A	area
acwl2	cowl taper angle
b	second coefficient in quadratic curve equation
b	second coefficient in equation for specific heat at constant pressure
c	third coefficient in quadratic curve equation
c	third coefficient in equation for specific heat at constant pressure
c_p	specific heat at constant pressure
c_v	specific heat at constant volume
d	fourth coefficient in equation for specific heat at constant pressure
dthcwl	delta change in cowl deflection angle
e	specific internal energy
e	fifth coefficient in equation for specific heat at constant pressure
E	E flux vector
F	F flux vector
h	static enthalpy

h_{in}	nozzle inlet height
h_{ex}	nozzle exit height
hcwl	cowl thickness
iparam	optimization parameter(s) flag
L	nozzle length
M	Mach number
P	static pressure
q	dynamic pressure
r	nozzle circular arc radius of curvature
R_{gas}	gas constant for mixture
tcwl2	cowl deflection angle
thcwl0	first temporary cowl deflection angle
thcwl1	second temporary cowl deflection angle
thcwl2	third temporary cowl deflection angle
T	static temperature
u	axial component of velocity
v	normal component of velocity
V	velocity magnitude
w	unit width
x	axial direction
x	nozzle attachment angle or cowl deflection angle in quadratic curve equation

xcwl1	first segment of cowl
xcwl2	second segment of cowl
y	normal direction
y	total thrust in quadratic curve equation

GREEK SYMBOLS

β	difference between shock wave angle and flow deflection angle
γ	specific heat ratio
δ	flow turning angle
$\Delta\zeta$	axial step size in transformed coordinate system
ε	shock wave angle
ζ	transformed axial coordinate
η	transformed normal coordinate
η_x	partial derivative of transformed normal coordinate with respect to x
η_y	partial derivative of transformed normal coordinate with respect to y
η_{KE}	inlet kinetic energy efficiency
θ	flow angle
θ_B	nozzle circular arc attachment angle
ρ	density
Ψ	general variable for Riemann problem

SUBSCRIPTS AND SUPERSCRIPTS

i	axial space direction index
j	normal space direction index
j+1/2	Riemann node between grid points j and j+1
o	initial condition
0, 1, 4, and 5	engine station designator corresponding to inlet entrance, diffuser entrance, combustor entrance, and combustor exit, respectively
0, 2, 4, or 6	Riemann region 0, 2, 4, or 6, respectively
1, 2	upstream or downstream of shock wave, respectively
1, 2, or 3	Riemann wave 1, 2, or 3, respectively

Abstract

An investigation of the effects of simultaneous variation of the nozzle attachment angle and cowl deflection angle on the performance of a two-dimensional nozzle used on a hypersonic vehicle such as the National Aero-Space Plane (NASP) was performed using a two parameter direct search optimization procedure. Total thrust optimization was accomplished using a Flux-Difference-Split (FDS) code, a RAMJET Performance Analysis (RJPA) program, and an oblique shock wave solver program, at sixteen points on a 1000 psf dynamic pressure trajectory for Mach numbers ranging from 10.0 to 25.0. A single parameter optimization of the total thrust using a variable nozzle attachment angle was accomplished first to establish a reference frame for comparison with the two parameter optimization results. Effects of a positively and negatively deflected cowl on the nozzle flow field were explored to provide the motivation to vary the cowl deflection angle along with the nozzle attachment angle. The positively deflected cowl increased the nozzle wall pressure, thus producing greater thrust but also producing greater pressure drag on the upper cowl wall. The optimum nozzle attachment and cowl deflection angle maximized the total thrust by increasing nozzle wall pressure without an excessive increase in pressure drag. The total thrust found by the two parameter optimization was increased at every point on the trajectory over the total thrust obtained from the single parameter optimization. This study shows that the cowl deflection angle starts negative, increasing from -0.493 degrees at Mach 10 to 3.01 degrees at Mach 25. The analysis

also shows that the nozzle attachment angle and cowl deflection angles are closely related to the nozzle entrance pressure and Mach angle. Increasing the length of the deflected cowl increased the total thrust of the configuration by causing the expansion to freestream to occur further from the nozzle entrance.

NOZZLE/COWL OPTIMIZATION FOR A HYPERSONIC VEHICLE ON A TYPICAL TRAJECTORY

I Introduction

1.1 Purpose

The purpose of this study was to investigate the effects of a two parameter direct search optimization of the nozzle attachment angle and cowl deflection angle on the performance of a two-dimensional nozzle used on a hypersonic vehicle such as the National Aero-Space Plane (NASP) (Figure 1-1), at various flight points on a typical trajectory. The total thrust produced by the nozzle/cowl configuration (Figure 1-2) was maximized by the optimization and compared to an established baseline total thrust.

1.2 Background

Hypersonic flight has received significant government interest through the National Aero-Space Plane (NASP) Program. In particular, the hypersonic propulsion problem is an area of research which has many facets. Extreme temperatures and thermal/mechanical stresses encountered in hypersonic flight press the limit of current material and cooling technologies. Thrust production is another key factor which presents demanding requirements. One aspect of the propulsion problem is the design of an optimized supersonic nozzle (Doty, 1991:1). Conventional propulsion systems are inadequate for hypersonic use because the air in the engine is slowed to subsonic speeds and therefore

the temperature of the air is increased greatly. Since the air temperature is high, the addition of combustion products to raise the temperature, and therefore the energy of the system, has little or no affect. This is caused by the dissociation of the combustion products at high temperatures and the fuel only helps the dissociation and does not produce thrust. Therefore, no useful thrust is produced if the air is slowed to subsonic speeds for combustion. For this reason, combustion at supersonic speed is required for thrust production in hypersonic flight. Supersonic combustion provides a wider thermal range where dissociation may be avoided. Thus, supersonic combustion ramjet (Scramjet) engines must replace the unfeasible conventional engines in the hypersonic speed regime.

According to Walton (1988:2), because of the extremely high Mach numbers that characterize flight in this speed regime, the resulting expansion at the afterbody can account for around 30 percent of the vehicle's thrust. For this reason, Scramjet nozzles tend to be long and highly integrated with the airframe of the vehicle (Henry and Anderson, 1973). However, Scramjet nozzles are extremely sensitive to changes in performance parameters. This sensitivity is exhibited in the limited research where dramatic changes in thrust are caused by slight changes in the ambient conditions. It is apparent that there can be little margin for error when designing a nozzle for optimum performance.

To obtain optimum performance, the hypersonic vehicle needs to fly within a prescribed envelope of altitude and flight speed as it transits the atmosphere. With this prescribed envelope, the flight and performance parameters can be maintained within useful limits as the vehicle conducts its mission. One of the parameters is the dynamic

pressure (q). Dynamic pressure is exclusively a function of the freestream conditions and can represent a trajectory frequently encountered in the literature for a NASP type vehicle (Billig, 1987:119). This parameter is selected for the proposed study and the vehicle is assumed to travel at the maximum q limit. The maximum q limit represents an effective design effort, employing state-of-the-art technology while minimizing overdesign. Overdesign is a major problem because excess weight would necessitate a larger engine and more fuel. Additional fuel would again increase the vehicle weight in an upward spiral that could result in a vehicle too large and too heavy to fly. Once again a slight change, such as an increase in fuel, could have a dramatic affect on the design which reinforces the need for an optimized nozzle.

1.3 Methodology

The technique and computer program recently implemented by Doty (1991) for the determination of maximum thrust planar nozzles provided the means of accomplishing this study. The Flux-Difference-Split (FDS) Method is a robust first order accurate method which is as good as most second order finite difference techniques (Taylor et al., 1972, Peyret et al., 1983). The FDS method is capable of handling complicated flow patterns which include interactions of shock waves, expansion waves, and contact surfaces. The few finite difference codes that can accomplish this task are extremely time consuming and costly to use (Doty, 1991:1), and are therefore not desirable for an optimization procedure. The optimization may require analysis of the entire flow field numerous times and the FDS code will give significant savings in computational time.

The basis of FDS method is the solution of the Riemann problem in one form or another (Godunov, 1959, Osher 1981, Pandolfi, 1985). The Riemann problem describes the local collapse of a discontinuity and the resulting fluxes. Once the Riemann problem is solved, the application of the FDS method is fairly straightforward and an entire flow field with numerous discontinuities may be determined. With the flow field determined, a direct two parameter optimization procedure will be employed. The coupling of the FDS method and the direct optimization procedure can design maximum thrust nozzles for a wide range of nozzle/cowl configurations.

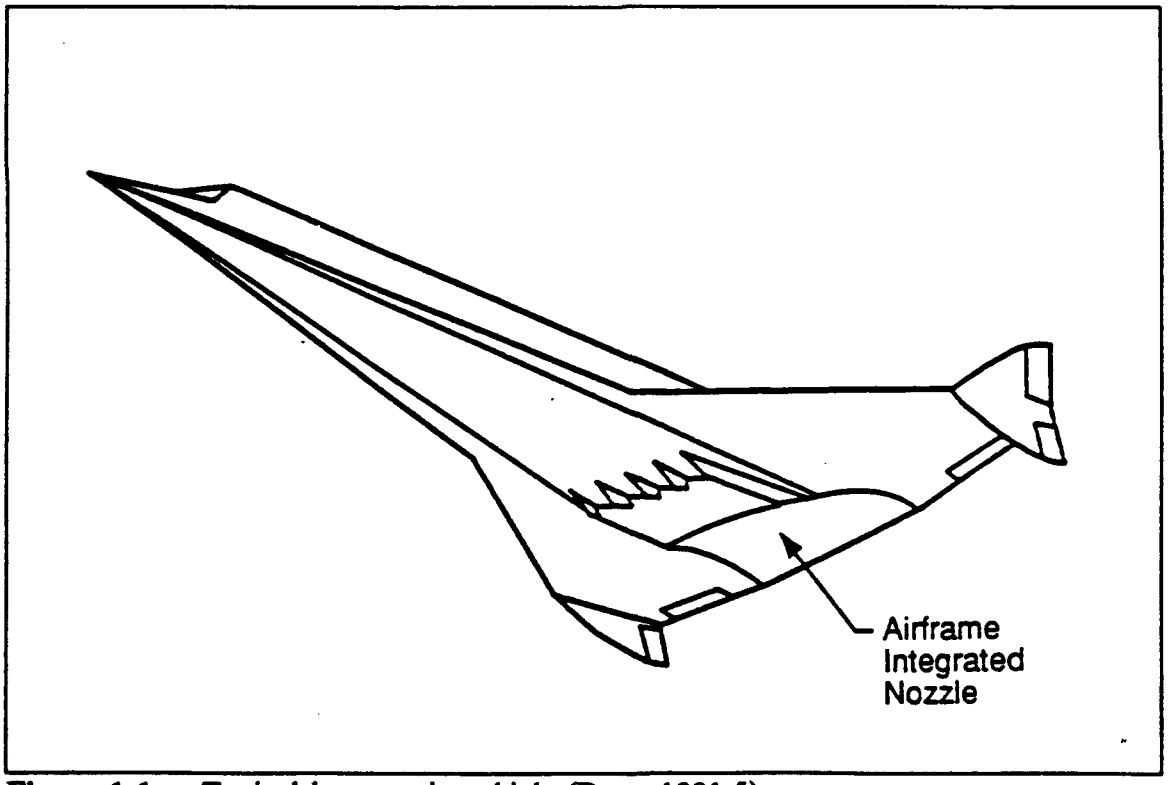

Figure 1-1 Typical hypersonic vehicle (Doty, 1991:5)

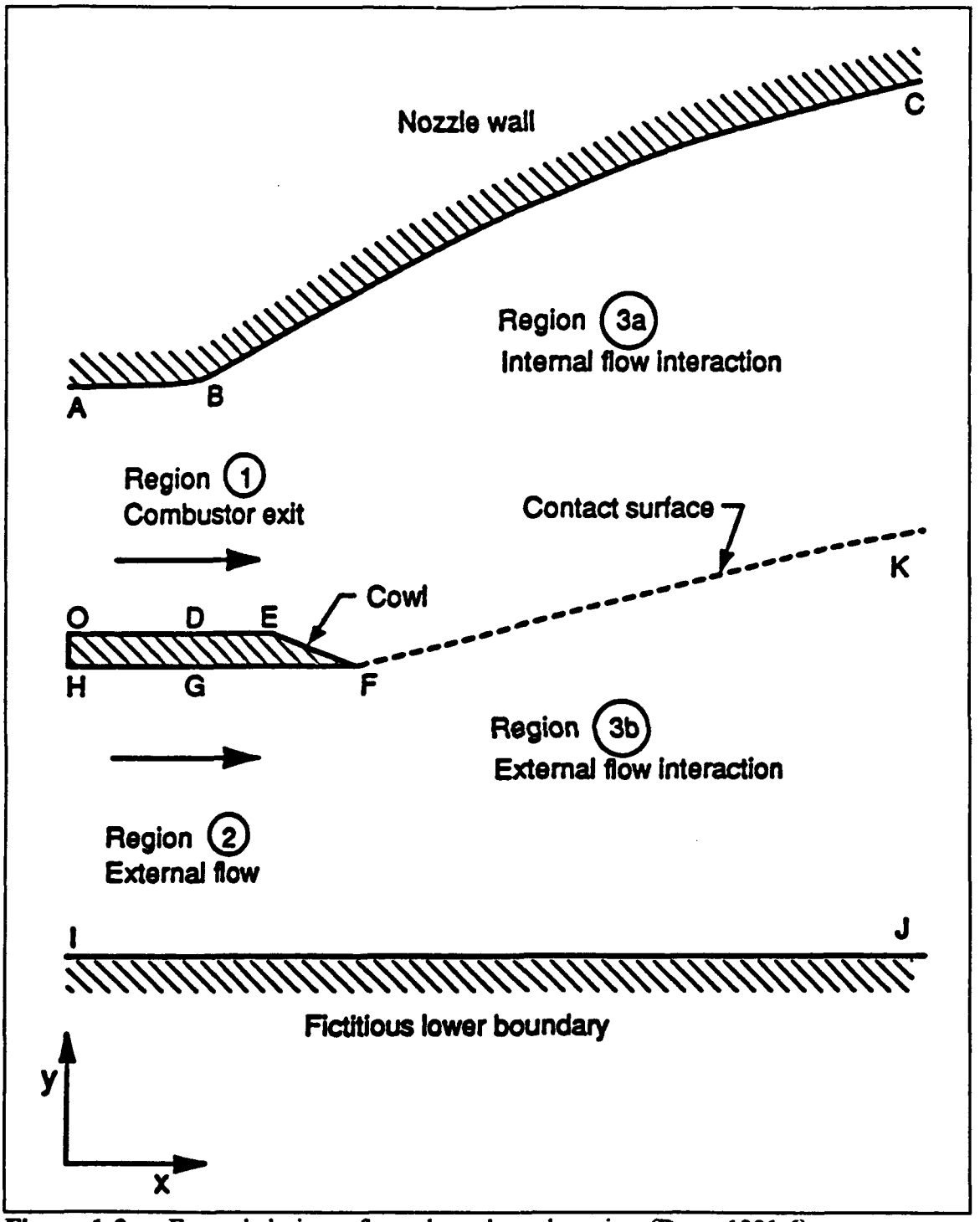

Figure 1-2 Expanded view of nozzle and cowl section (Doty, 1991:6)

II Analytic Development and Methodology

2.1 Governing Equations (Doty,1991:Ch 2)

The governing equations of motion for a planar, steady, adiabatic, inviscid flow of a compressible fluid with no external work or body forces are the Euler equations of fluid dynamics. In vector divergence form, those equations are:

$$\frac{\partial E}{\partial x} + \frac{\partial F}{\partial y} = 0 \qquad \textbf{(2-1)}$$

where the **E** and **F** vectors are written in terms of the conservation variables as

$$E = \begin{bmatrix} \rho u \\ \rho u^2 + P \\ \rho uv \\ u\,(\rho e + P) \end{bmatrix} \qquad F = \begin{bmatrix} \rho v \\ \rho vu \\ \rho v^2 + P \\ v\,(\rho e + P) \end{bmatrix} \qquad \textbf{(2-2)}$$

The first of Eqs (2-2) is the continuity equation, the second and third are the axial and radial momentum equations, respectively, and the fourth is the energy equation.

2.1.1 Thermodynamic Model

The equations of state chosen for the analysis are those of a thermally and calorically perfect gas. The equation of state for a thermally perfect gas is:

$$T = \frac{P}{\rho R_{gas}} \qquad \textbf{(2-3)}$$

while for a calorically perfect gas, the total specific internal energy is given by:

$$\rho e = \frac{P}{\gamma - 1} + \frac{1}{2} \rho (u^2 + v^2) \qquad \textbf{(2-4)}$$

2.2 Coordinate Transformation

The numerical solution is carried out in uniform orthogonal computational space. Transformation of the governing equations into the computational space is required. Equation (2-1) is transformed as:

$$\frac{\partial E}{\partial \zeta} = - \eta_x \frac{\partial E}{\partial \eta} - \eta_y \frac{\partial F}{\partial \eta} \qquad \textbf{(2-5)}$$

where ζ and η are the transformed coordinates, and η_x and η_y are the transformation metrics (Doty, 1991:Appendix G).

2.3 Numerical Algorithm

This study used a Flux Difference Split (FDS) code developed by Doty (1991) to solve the nozzle flow field. The FDS method relies on the Riemann problem, the solution of a discontinuity. The wave-like nature of the Riemann problem is used to split the solution of the Riemann problem along the preferred paths of information propagation (Doty, 1991:153). Discontinuities such as shock waves are processed and the numerical solution is calculated using the processed information.

The Riemann problem is represented in Figure 2-1. The general flow property,

Ψ, has an arbitrary spatial distribution represented by the solid line. The flow property can be modeled as distinct, uniform regions (Godunov, 1959) represented by the dashed line. The adjacent boundary is assumed to occur half-way between where the flow properties are known (points (j) and (j+1)).

Collapse of the discontinuity between regions produces the possible wave pattern shown is Figure 2-2. Waves (1) and (3) may each be a compression (shock) wave or expansion wave and are referred to as the negative and positive wave, respectively, because of the direction the wave carries information. Wave (2) is the contact surface which separates the Riemann regions. The notation for the Riemann problem between grid points j and j+1, illustrated in Figure 2-2, is as follows:

Riemann region 6 = known values at grid point "j+1"
Riemann region 4 = unknown values at midpoint "j+1/2"
Riemann region 2 = unknown values at midpoint "j+1/2"
Riemann region 0 = known values at grid point "j"

Similar notation is used for other pairs of grid points by permuting the indices.

The solution of the Riemann problem provides the flow properties in regions 2 and 4, Figure 2-2, along with the numerical fluxes based on the governing equations. For this study, an approximate Riemann problem was solved using linearized versions of the Prandtl-Meyer relations (Pandolfi, 1985). The FDS method differences the fluxes and then splits them into positive and negative portions, sending the information in the correct direction. For more information concerning the FDS method and the Riemann problem, refer to Doty (1991).

2.4 Thrust Calculation

After the flow field for the nozzle geometry has been analyzed with the FDS method, the flow properties are known. Thrust for the planar geometry is based on pressure acting on an area and is calculated using the following relation:

$$Thrust = \int P \, dA \tag{2-6}$$

where P is the pressure and dA is the incremental area. Since the nozzle is two-dimensional, the area can be represented by the height, y, multiplied by a unit width, w, resulting in the thrust per unit width given by:

$$\frac{Thrust}{w} = \int_{y_1}^{y_2} P \, dy \tag{2-7}$$

The sum of the thrust contributions from the nozzle, upper cowl, and lower cowl walls represents the total thrust of the nozzle/cowl configuration.

2.5 Optimization Process

The nozzle attachment angle, θ_B (Figure 2-3), and cowl deflection angle, tcwl2 (Figure 2-4) were used to optimize the total thrust of the nozzle/cowl assembly (Figure 1-2). The optimization procedure used in this study was a two parameter direct search method. The underlying structure of the two parameter search is similar to the single parameter direct search method used by Doty (1991). With the two parameter direct search, a direct search is accomplished on the first parameter, the nozzle attachment angle, while holding the second parameter, the cowl deflection angle, constant.

Figure 2-5 represents several thrust curves based on a variable nozzle attachment angle with constant cowl deflection angles. The object of the first search was to locate a nozzle attachment angle near the maximum of one of the curves in Figure 2-5. Next, a direct search is completed on the cowl deflection angle with the new nozzle attachment angle being held constant, represented by the verticle dashed line in Figure 2-5. By varying the cowl deflection angle, movement between the thrust curves to find a new cowl deflection angle and maximum thrust is possible. With the new cowl deflection angle, the procedure is repeated until the maximum total thrust of the nozzle/cowl assembly is determined.

Each direct search is based on analysis of three data points using a quadratic curve fit to determine a local maximum (see Figure 2-6). The three data points represent either the nozzle attachment angle or cowl deflection angle and the associated thrust. The quadratic curve is an approximation of the thrust based on the nozzle attachment angle, Figure 2-7, or the cowl deflection angle, Figure 2-8. The maximum is determined by analysis of the first and second derivatives of the quadratic curve. The quadratic curve is given by:

$$y = a + b\,x + c\,x^2 \qquad \textbf{(2-8)}$$

where y represents the total thrust and x represents either the nozzle attachment angle or the cowl deflection angle. For each of the three data points illustrated in Figure 2-6, the quadratic equation given by Eq 2-8 is valid. Thus, the coefficients, a, b, and c, are determined by solving the following system of equations:

$$\begin{bmatrix} 1 & x_1 & x_1^2 \\ 1 & x_2 & x_2^2 \\ 1 & x_3 & x_3^2 \end{bmatrix} \begin{bmatrix} a \\ b \\ c \end{bmatrix} = \begin{bmatrix} y_1 \\ y_2 \\ y_3 \end{bmatrix} \tag{2-9}$$

By using Gaussian elimination, a, b, and c are solved for and easily programmed using the following equations:

$$a = y_1 - b\,x_1 - c\,x_1^2 \tag{2-10}$$

$$b = \frac{(y_2 - y_1) - (x_2^2 - x_1^2)\,c}{x_2 - x_1} \tag{2-11}$$

$$c = \frac{(y_3 - y_1) - (y_2 - y_1)\,\dfrac{x_3 - x_1}{x_2 - x_1}}{(x_3^2 - x_1^2) - (x_2^2 - x_1^2)\,\dfrac{x_3 - x_1}{x_2 - x_1}} \tag{2-12}$$

To find the value of the nozzle attachment angle, x, yielding maximum total thrust, y, the first derivative of Eq (2-8), in equation form, is set to zero.

$$\frac{d\,y}{d\,x} = b + 2\,c\,x = 0 \tag{2-13}$$

Solving the right portion of Eq (2-13) for the nozzle attachment angle, x, a new value is

calculated with the previously determined coefficients with the following:

$$x = -\frac{b}{2c} \tag{2-14}$$

To insure a maximum is found, instead of a minimum, the second derivative of Eq (2-8), determined by

$$\frac{d^2 y}{d x^2} = 2c \tag{2-15}$$

is tested to be positive or negative. If positive, the nozzle attachment angle is at the minimum and therefore not the value wanted. The dashed line in Figure 2-9 represents a quadratic curve with a positive second derivative and the computed angle at the minimum. The maximum of the thrust curve, illustrated by the solid line in Figure 2-9, is on the opposite side of the data points from the computed angle. Figure 2-9 shows that a new value of the nozzle attachment angle is found by projecting the computed value to the opposite side of the data points. In the case presented by Figure 2-7, the thrust curve near the maximum contains an inflection point which would cause the quadratic curve fit with a positive second derivative. Although the optimal value may be passed over, the projected value keeps the process from wandering too far away from the goal of the optimal value.

After the new nozzle attachment angle is determined, the total thrust is then determined with the same method that determined the three initial data points. The absolute error of the new total thrust and that of the first data point is checked against an error tolerance to determine if convergence has been reached. The absolute error is given

by:

$$abs\left(\frac{y_{new} - y_1}{y_{new}}\right) \leq tolerance_y \qquad \textbf{(2-16)}$$

After convergence, the nozzle/cowl performance characteristics are saved in an output file.

2.6 Parameter Selection - Initial Values

Four combinations of the nozzle attachment and cowl deflection angles were tested to insure the procedure converged on the set of angles which produced maximum thrust. The four combinations were chosen to reflect combinations of angles both greater than and less than the optimum angles as follows:

$\theta_B > \theta_{opt}$ and tcwl2 > $tcwl2_{opt}$
$\theta_B < \theta_{opt}$ and tcwl2 < $tcwl2_{opt}$
$\theta_B < \theta_{opt}$ and tcwl2 > $tcwl2_{opt}$
$\theta_B > \theta_{opt}$ and tcwl2 < $tcwl2_{opt}$

All values during convergence were recorded for each combination and collected for analysis. If more than one set of information was obtained for the same nozzle attachment angle, only the data set which produced the highest thrust value was retained for analysis.

2.7 Code Modifications

The incorporation of the two parameter direct search procedure into the nozzle analysis program was a relatively straightforward task. The program was set up with a one parameter optimization. A second set of three independent variables were patterned

after the original set. The same dependent variable, total thrust, was used since the purpose was to maximize that value by changing both of the independent variables, the nozzle attachment angle and the cowl deflection angle.

As mentioned in Section 2.5, while the nozzle attachment angle is used in the optimization, the cowl deflection angle is held constant and vice versa. After the second, single direct search logic was added to the code, a flag was set up to alternate between the two single parameter searches. Also, the values of the nozzle attachment angle and the cowl deflection angle that determine the highest value of total thrust are stored in case the procedure finds a local plateau in the curve instead of the maximum (Figure 2-10). These stored parameters then are used after convergence on the plateau to obtain a maximum value of total thrust.

The input file was altered to include a choice for either a one or two parameter optimization. The flag, iparam, is set to 1 for the single parameter optimization and 2 for the two parameter optimization. Also a delta change variable, dthcwl, on the cowl deflection angle is available to give the user control over the second and third value of the cowl deflection angle.

Two common blocks were added. The first block holds the flags that control whether one or two parameter optimization was chosen. The second contains the three temporary values; thcwl1, thcwl2, and thcwl0; of the cowl deflection angle and the delta change variable, dthcwl, mentioned above.

Since the code was initially set up to make the cowl wall, Figure 2-4, only once, modification to the cowl wall generator was required. The change in the cowl wall

generator consisted of deactivating the consolidation of parallel sections. In Figure 2-4, xcwl1 and xcwl2 would be combined into xcwl1, with xcwl2 set to zero when the angle tcwl2 was zero. Subsequent cowl wall generation would produce only a straight cowl, nullifying the cowl deflection angle, tcwl2.

Since the optimization changes the cowl deflection angle, tcwl2, generation of a new cowl wall was needed for each new angle used. The new cowl wall is needed to properly represent the interior and exterior flow fields necessary for the calculation of the total thrust.

Another modification was required within the flow field analysis portion of the code. With the original code, the initial value line, dashed line from H to I, for the external flow (see Figure 1-2) was moved from point H under the nozzle entrance to the far end of the cowl, point F, since the cowl remained fixed. With the variable cowl, the initial value line must remain under the nozzle entrance, point H, to insure the proper effects of the cowl on the interior and exterior flows.

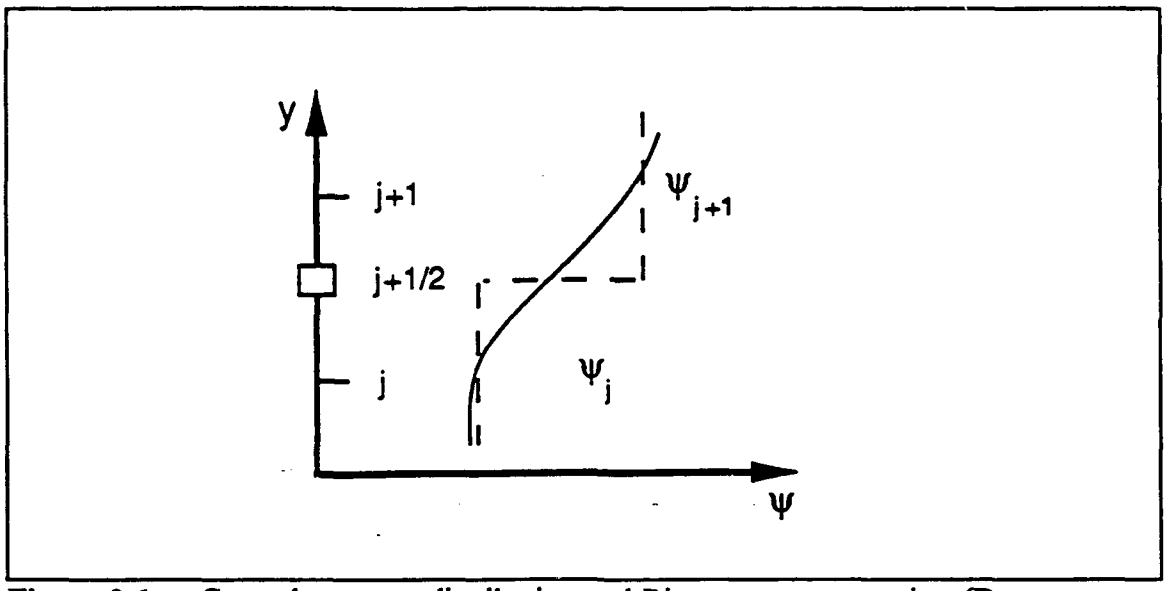

Figure 2-1 General property distribution and Riemann representation (Doty, 1991:16)

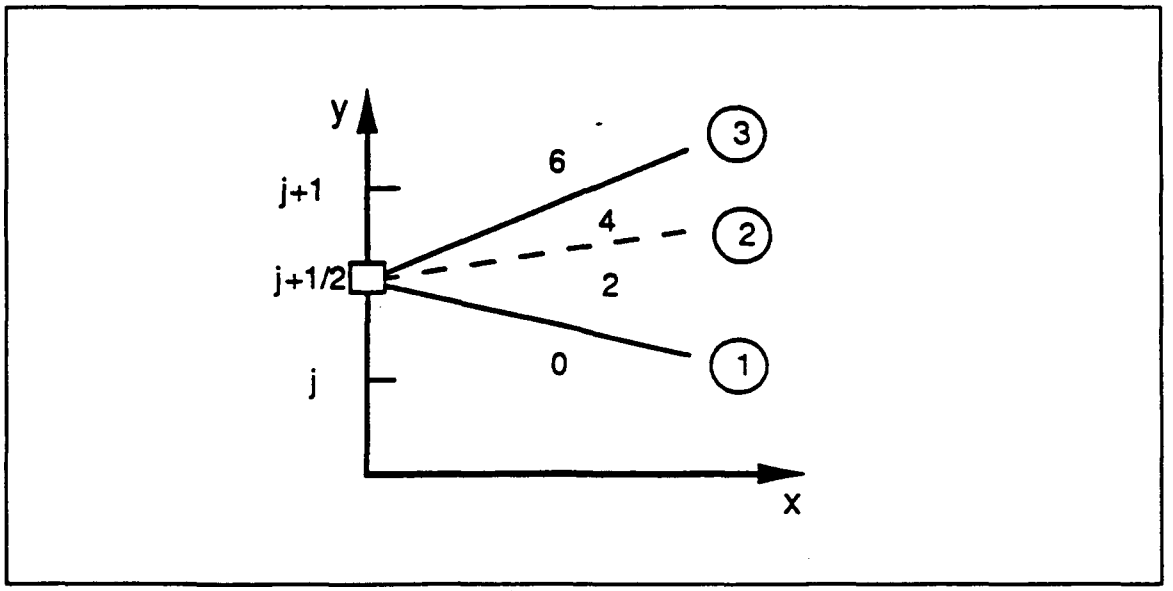

Figure 2-2 Riemann wave pattern (Doty, 1991:174)

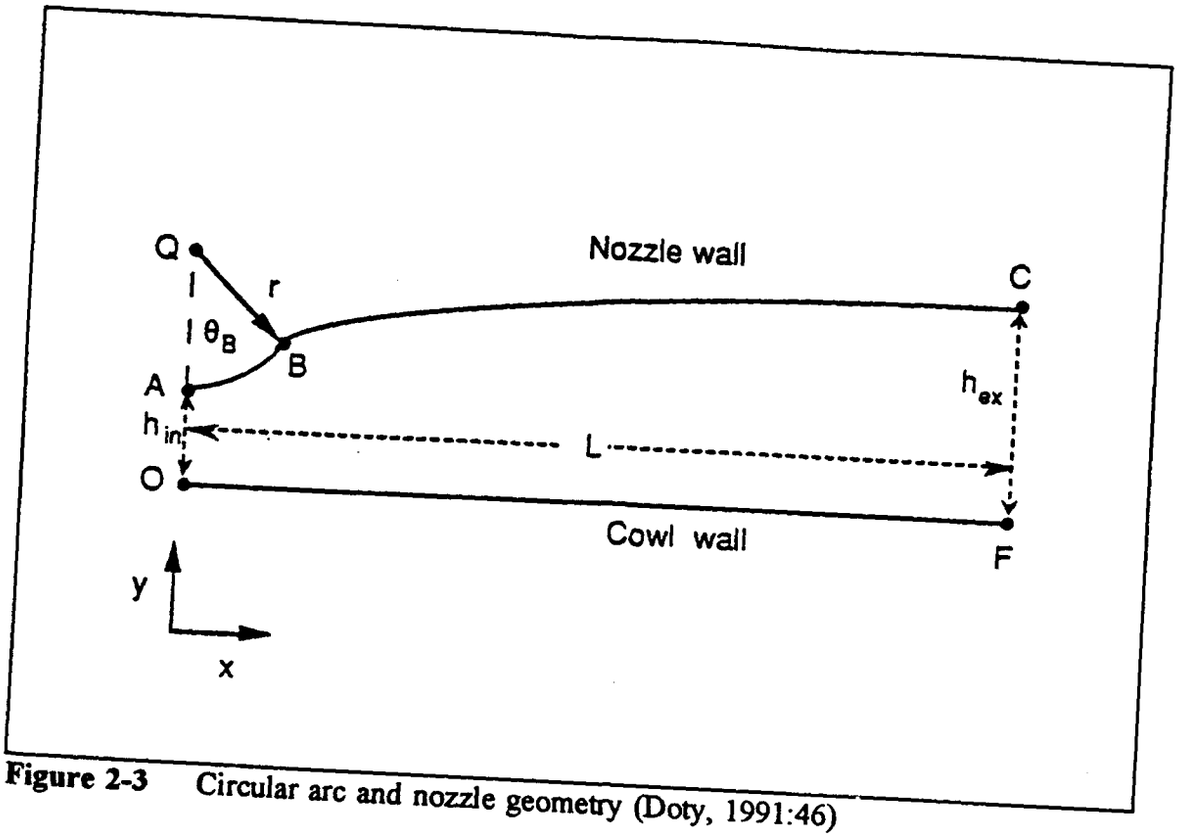

Figure 2-3 Circular arc and nozzle geometry (Doty, 1991:46)

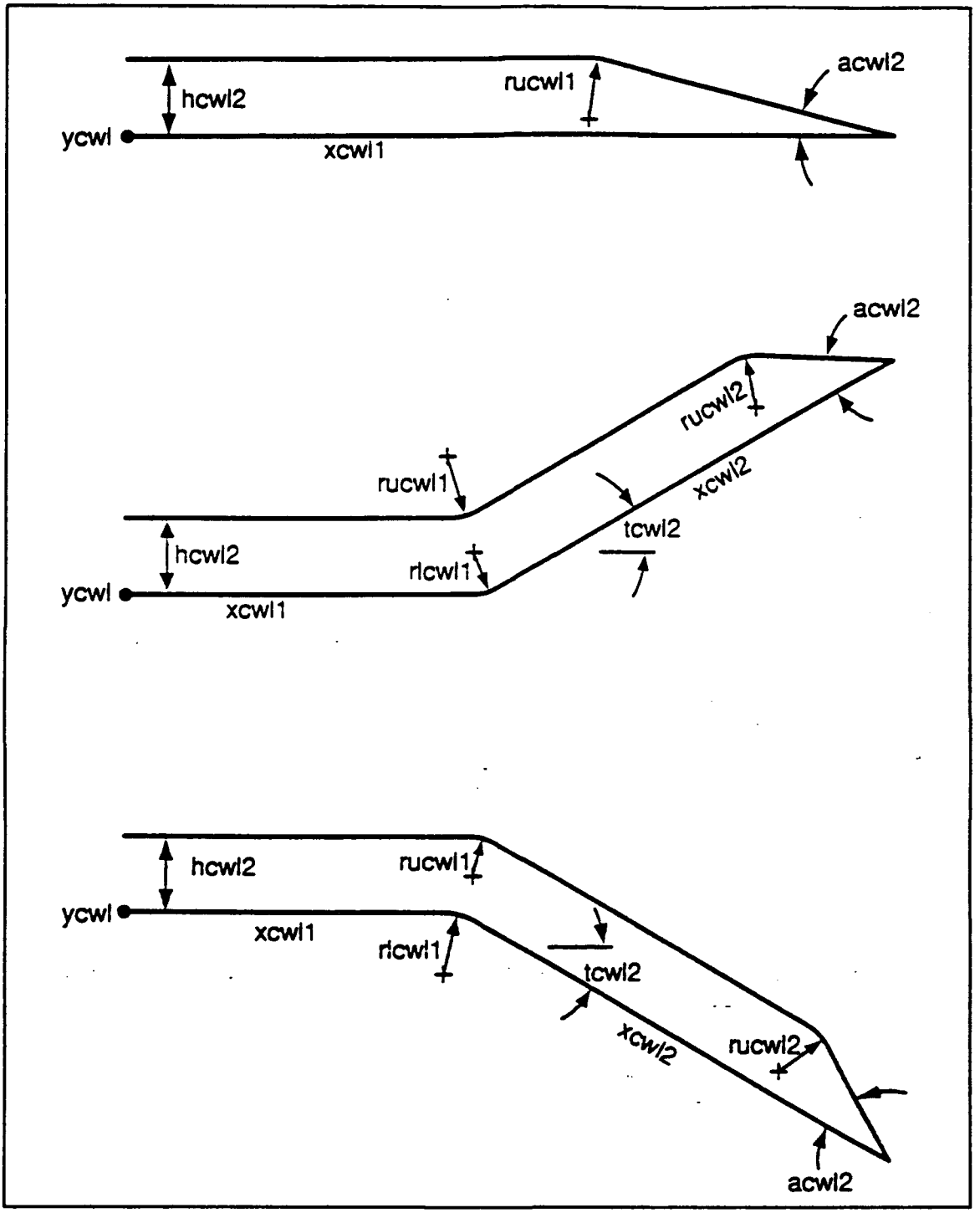

Figure 2-4 Examples of possible cowl configurations (Doty, 1991:231)

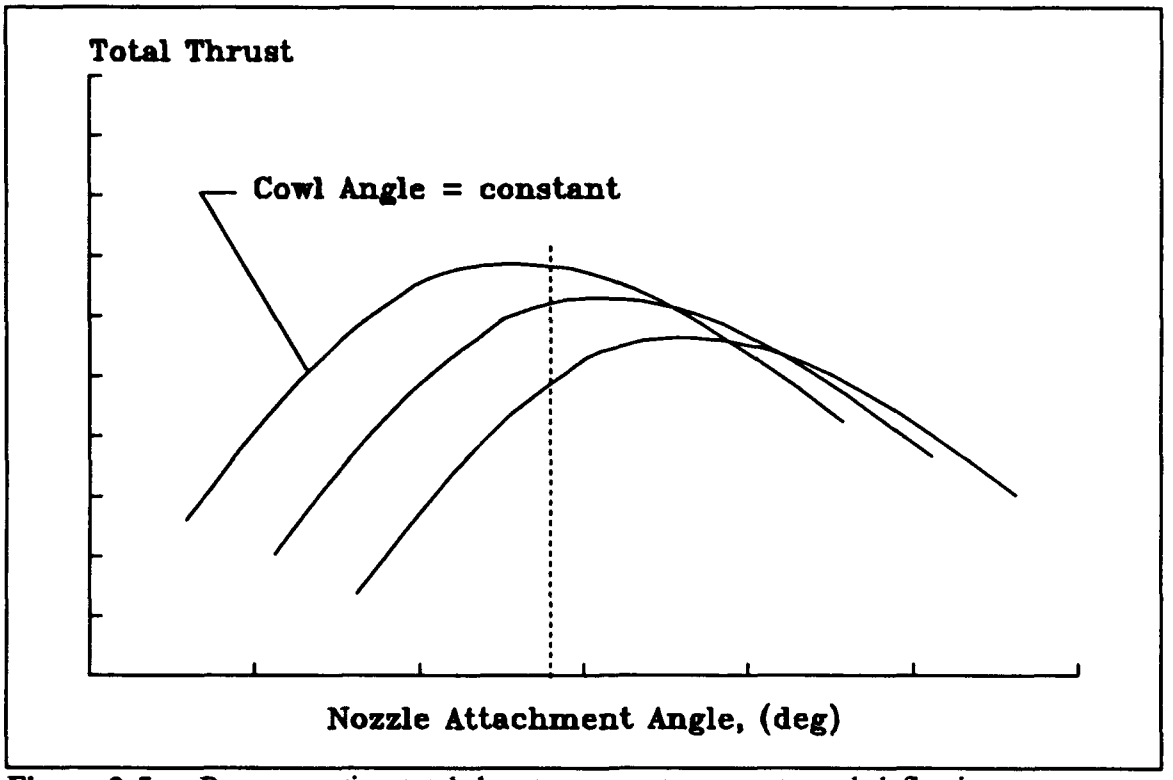

Figure 2-5 Representative total thrust curves at constant cowl deflection

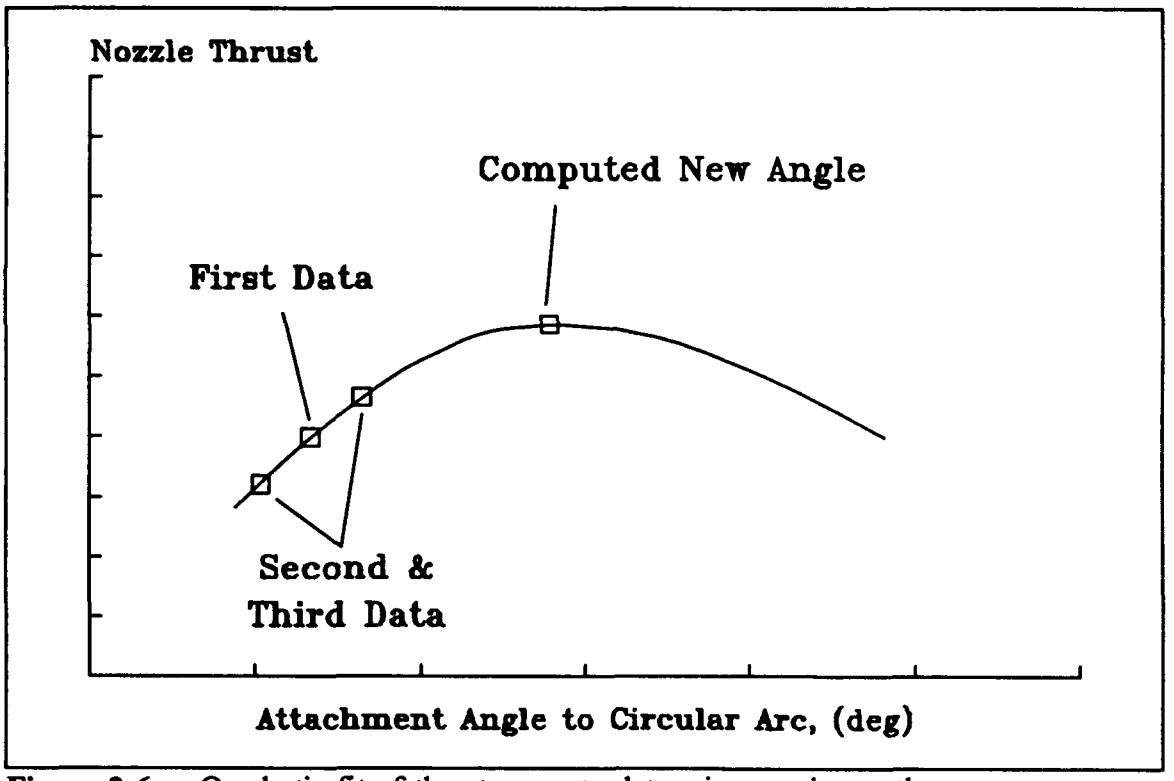

Figure 2-6 Quadratic fit of thrust curve to determine maximum thrust

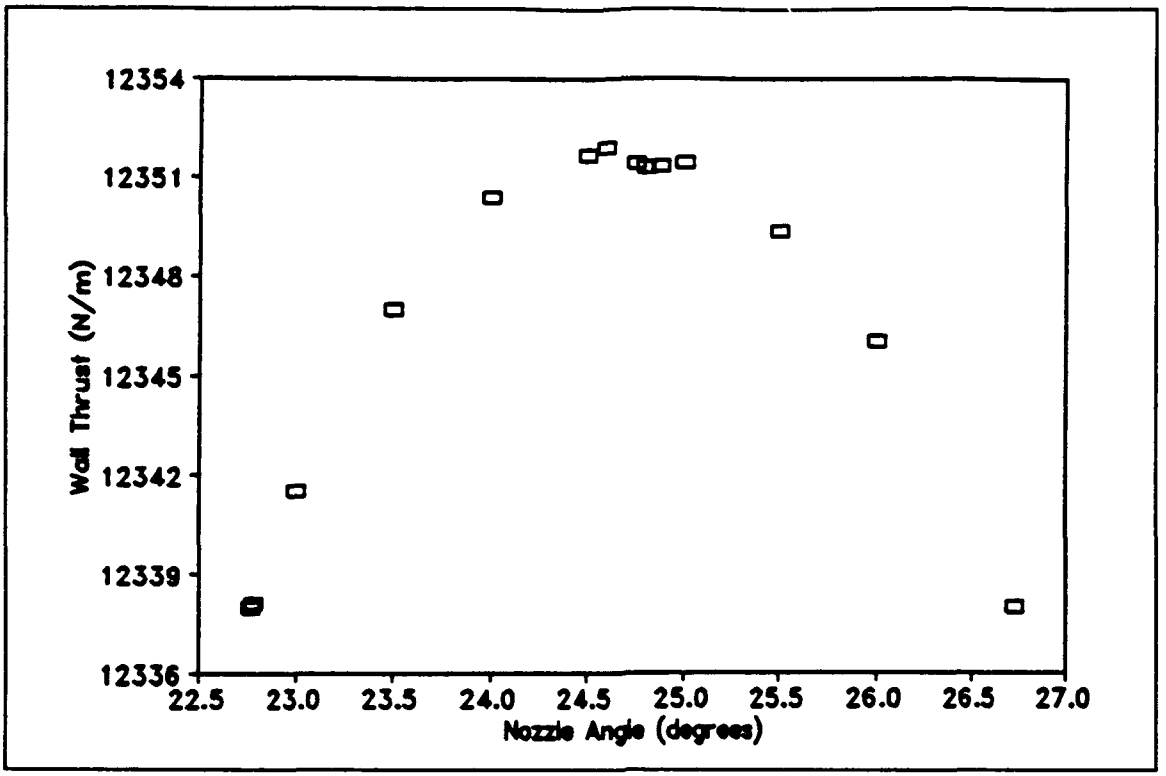

Figure 2-7 The effect of nozzle attachment angle on wall thrust for Mach number 15.0 (Herring, 1991:90)

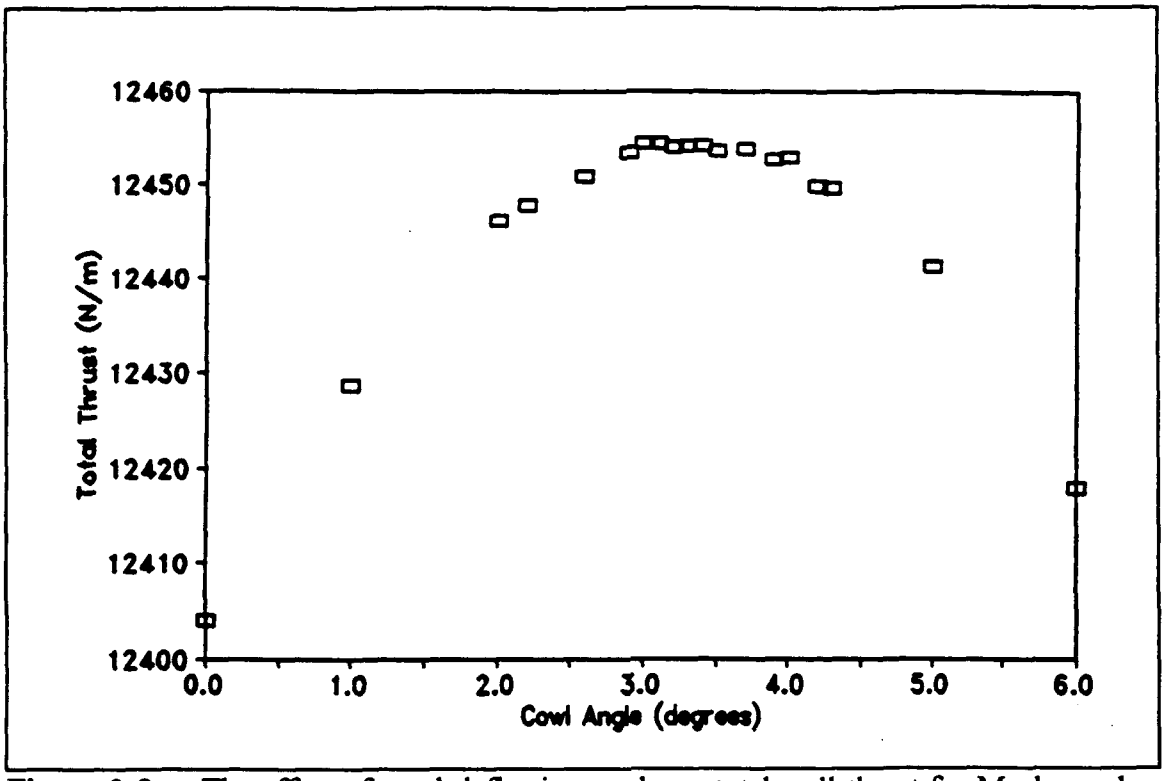

Figure 2-8 The effect of cowl deflection angle on total wall thrust for Mach number 15.0 and nozzle attachment angle 20.6 degrees (Herring, 1991:98)

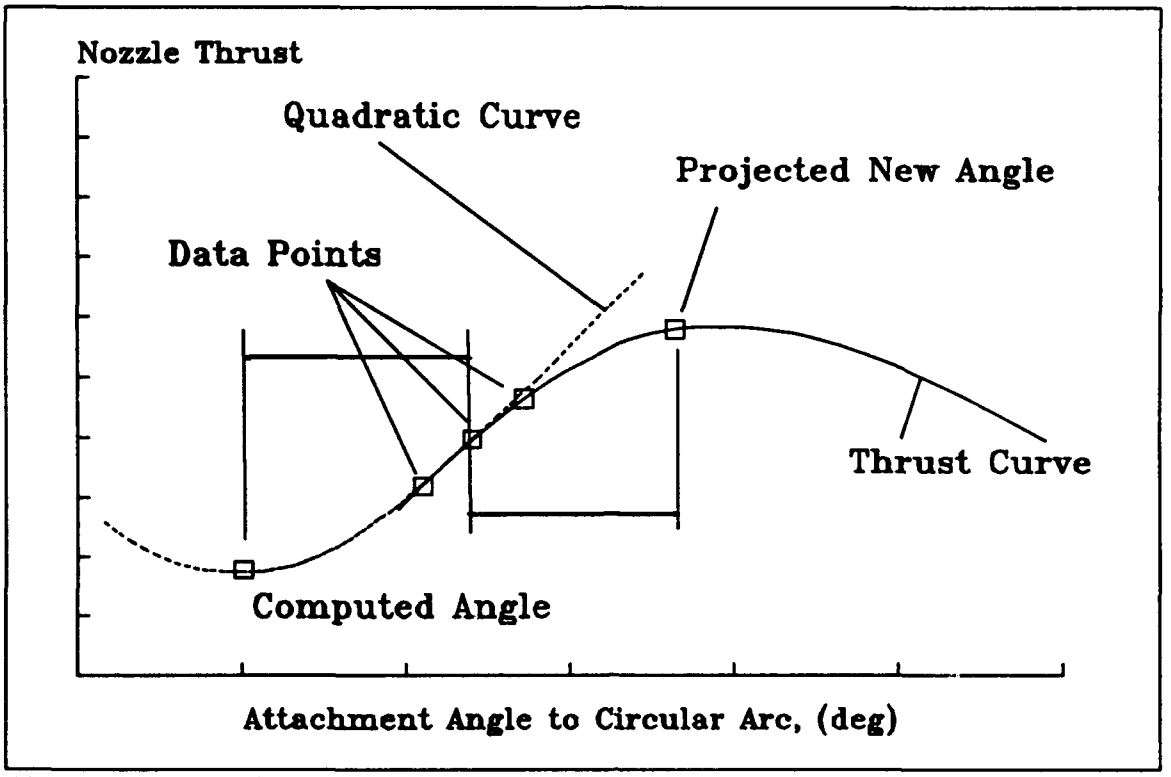

Figure 2-9 Angle on quadratic curve at minimum value projected toward maximum thrust value

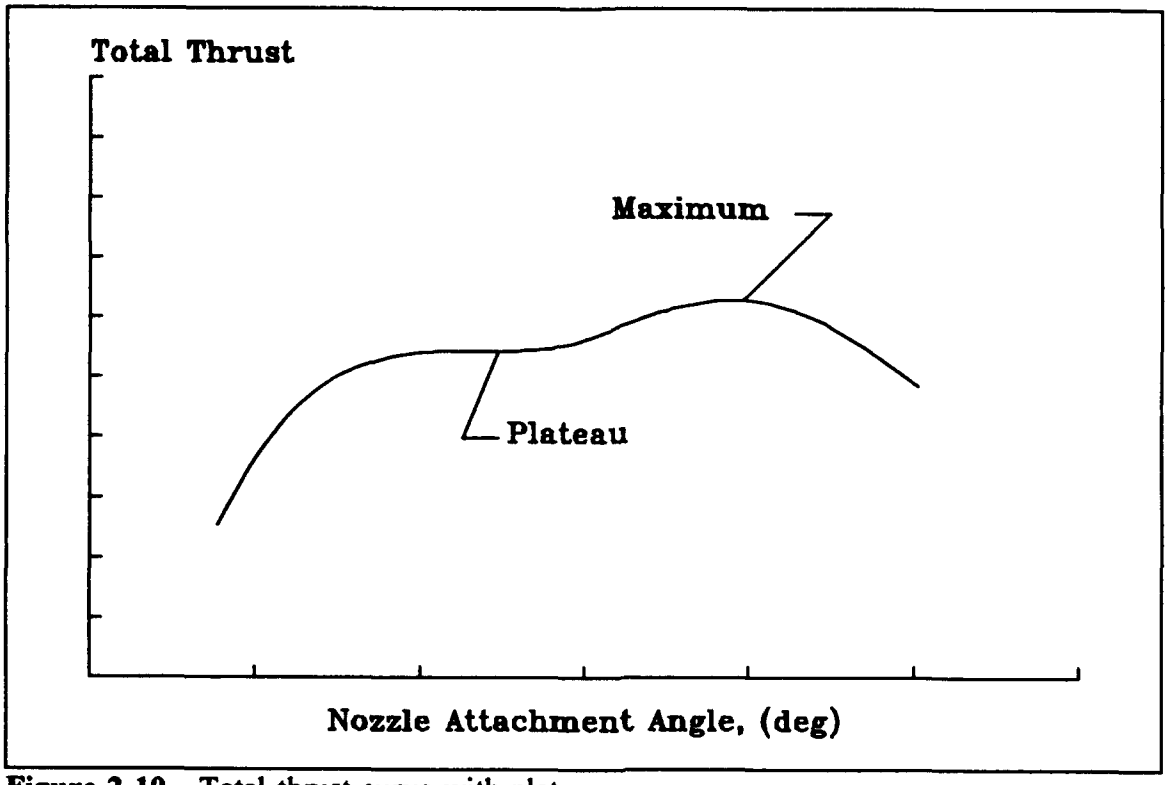

Figure 2-10 Total thrust curve with plateau

III Preliminary Procedure

3.1 The Trajectory

A hypersonic vehicle will typically travel along a predetermined path. Such a path can be determined by using a constant dynamic pressure, q, to represent aerodynamic and structural loads of the vehicle. A typical value of dynamic pressure for a NASP-type vehicle is q = 1000 psf (Billig, 1987:119).

By definition, the dynamic pressure is exclusively a function of the freestream conditions:

$$q_\infty = \frac{1}{2} \rho_\infty V_\infty^2 \tag{3-1}$$

In a more useful form, the velocity is expressed in terms of the Mach number and speed of sound:

$$V^2 = M^2 a^2 \tag{3-2}$$

where the speed of sound of a perfect gas is:

$$a^2 = \frac{\gamma P}{\rho} \tag{3-3}$$

When equations (3-2) and (3-3) are substituted into equation (3-1) and simplified, the following is obtained

$$q_\infty = \frac{1}{2} \gamma P_\infty M_\infty^2 \qquad \textbf{(3-4)}$$

Solving Eq (3-4) for the freestream pressure gives

$$P_\infty = \frac{2 q_\infty}{\gamma M_\infty^2} \qquad \textbf{(3-5)}$$

For a given dynamic pressure and specific heat ratio, Eq (3-5) gives the freestream pressure as a function of Mach Number. With the calculated pressure, the altitude was determined from established data such as the 1976 US Standard Atmosphere Tables (US COESA, 1976). Figure 3-1 shows the relationship between Mach number and altitude for a constant dynamic pressure, q = 1000 psf. The other freestream conditions were obtained from the RamJet Performance Analysis (RJPA) Program (Pandolfini, 1986) by specifying the altitude and Mach number as inputs. Details of RJPA are presented in Section 3.2. Table 3-1 provides the freestream properties for the trajectory from Mach 10 to 25. Since the freestream is undisturbed, the static temperature and pressure are modeled well by the thermally and calorically perfect gas. For this reason, the specific heat ratio and gas constant are assumed fixed to the values in Table 3-1.

Table 3-1 Freestream flow conditions at each trajectory point

Mach Number	Altitude, (m)	Static Pressure, P (N/m^2)	Static Temperature T (K)	Density, ρ (kg/m^3)	Velocity Magnitude, V (m/s)	Specific Heat Ratio, γ	Gas Constant, R_g (J/kg/K)
10.0	33802	682.73	233.20	1.0201e-02	3070.9	1.4	287.0
11.0	35113	565.46	236.83	8.3194e-03	3403.9	1.4	287.0
12.0	36332	475.80	240.20	6.9017e-03	3739.4	1.4	287.0
13.0	37490	404.72	243.41	5.7934e-03	4077.7	1.4	287.0
14.0	38557	349.38	246.36	4.9414e-03	4417.6	1.4	287.0
15.0	39594	303.39	249.22	4.2415e-03	4760.2	1.4	287.0
16.0	40538	267.14	251.84	3.6959e-03	5103.8	1.4	287.0
17.0	41453	236.49	254.37	3.2394e-03	5449.5	1.4	287.0
18.0	42306	211.31	256.72	2.8680e-03	5796.4	1.4	287.0
19.0	43129	189.76	259.00	2.5528e-03	6145.0	1.4	287.0
20.0	43922	171.24	261.19	2.2844e-03	6495.3	1.4	287.0
21.0	44684	155.27	263.29	2.0548e-03	6847.1	1.4	287.0
22.0	45415	141.45	265.31	1.8576e-03	7200.2	1.4	287.0
23.0	46116	129.45	267.24	1.6877e-03	7554.4	1.4	287.0
24.0	46817	118.54	269.18	1.5343e-03	7910.9	1.4	287.0
25.0	47457	109.44	270.65	1.4089e-03	8262.6	1.4	287.0

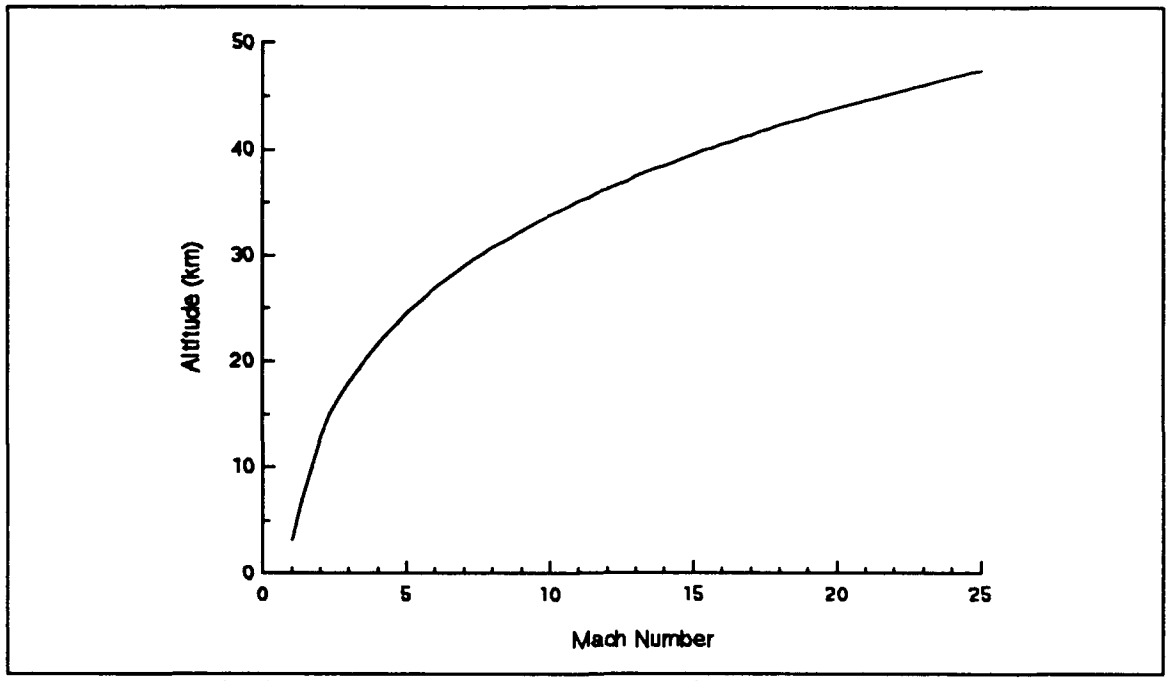

Figure 3-1 The hypersonic trajectory. The relationship between Mach number and altitude for a constant dynamic pressure, q = 1000 psf

3.2 Internal Flow - Ramjet Performance Analysis Program

To evaluate the trends of the nozzle/cowl configuration over the trajectory, the flow properties entering the nozzle should be consistent with scramjet combustor exit conditions over the trajectory. Since the purpose of this study is focused on the nozzle, the combustor exit flow conditions were assumed to be uniform and the result of supersonic combustion of fuel and air within a Scramjet engine. The model of the Scramjet engine used was a computer program developed by the Johns Hopkins University; the RamJet Performance Analysis (RJPA) IBM-PC version 1.0 (Pandolfini, 1986).

RJPA is a one-dimensional integral simulation code and requires two files: a setup

file and a thermochemical data file. The setup file contains all the parameters RJPA needs to set up the engine specifications. The thermochemical data file holds all information required for the equilibrium chemistry calculations (Pandolfini, 1986). The results of the simulation from the freestream to the exit of the combustor are used as the initial conditions for the nozzle flow field calculations.

3.2.1 RamJet Performance Analysis Assumptions and Input Parameters

Several assumptions were made in specifying the input parameters for the engine and the cycle analysis. The instruction manual for RJPA provides the necessary information to construct (or modify) an input file (Pandolfini, 1986). Example 1 in the manual was used as a guide in constructing files for each point on the trajectory. The following list provides an overview of the important parameters in the input file.

1. The inlet reference area was defined as 100 ft^2, constant over the entire trajectory.
2. The inlet capture area ratio was assumed to have a linear dependence based on the freestream Mach number. At the low Mach number, the inlet was assumed to be less than optimal, Table 3-2, and at the high Mach number to be optimal.

Table 3-2 Inlet capture area ratio extremes

M_∞	A_o / A_i
3.0	0.5
25.0	1.0

From the values in Table 3-2, a linear dependence of the inlet capture area ratio

based on the freestream Mach number was determined as the following:

$$\frac{A_o}{A_i}(M_\infty) = 0.4318 + 0.0227\, M_\infty \qquad \textbf{(3-6)}$$

3. The inlet contraction ratio was also assumed to have a linear dependence based on the freestream Mach number to provide the diffuser exit area. Table 3-3 displays the assumed extremes.

Table 3-3 Inlet contraction ratio extremes

M_∞	A_o / A_4
3.0	3.0
25.0	50.0

Based on the values in Table 3-3, a linear dependence was determined as the following:

$$\frac{A_o}{A_4}(M_\infty) = -3.41 + 2.136\, M_\infty \qquad \textbf{(3-7)}$$

4. The inlet efficiency was accounted for with the kinetic energy efficiency parameter η_{KE}. The value found in Example 1 of the RJPA manual was used and held constant over the trajectory

5. The combustor exit area was assumed to be the sum of the diffuser exit area plus a gas generator area since the constant area option of RJPA was used. The gas generator area was assumed to be five percent of the diffuser exit area value to provide RJPA with sufficient data to complete the cycle analysis.

6. The stoichiometric fuel/air ratio for a hydrogen-air combustion process was used. To reduce the number of variables, the ratio was held constant over the trajectory.

3.2.2 RJPA Output

The output file contains flow conditions and equilibrium composition at each station in the ramjet cycle (Figure 3-2). Only the combustor exit flow conditions were required to set up the initial value line for the internal nozzle portion of the FDS code (Doty, 1991:40). The important flow properties obtained were the static pressure, static temperature, density, flow Mach number, specific heat ratio, and molecular weight. Table 3-4 contains these data for each point on the trajectory. The specific heat ratio and mixture gas constant varied over the trajectory points but were held at $\gamma = 1.25$ and $R = 375$ J/kg/K to reduce the number of variable parameters in the nozzle analysis. As mentioned before, similar flow properties were obtained for the freestream from the portion of the output which contained the inlet entrance data and are summarized in Table 3-1.

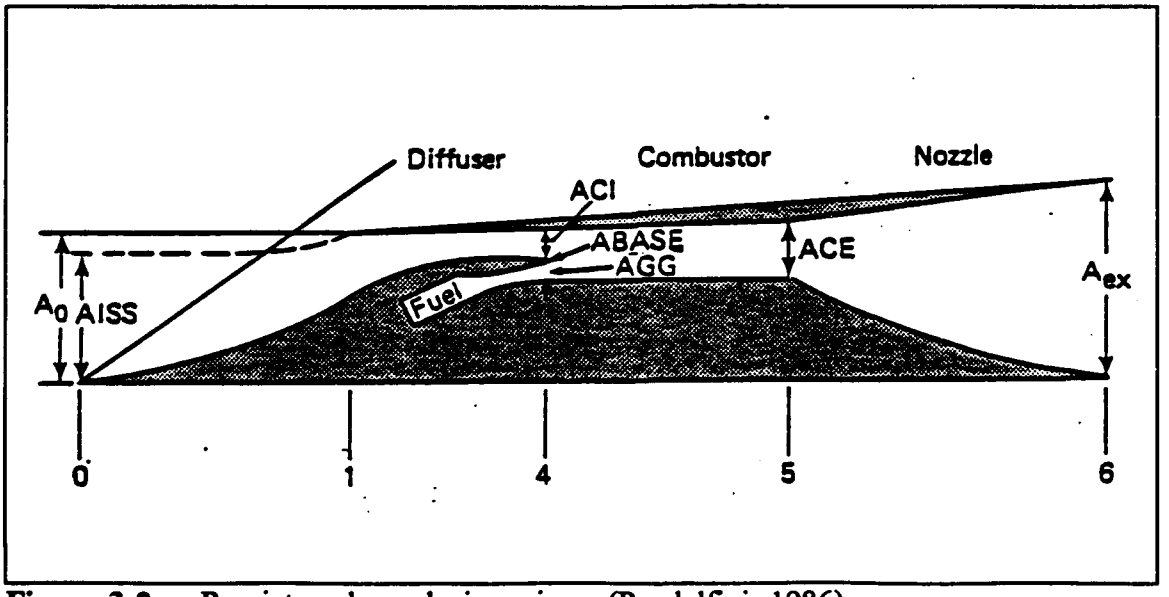

Figure 3-2 Ramjet cycle analysis regimes (Pandolfini, 1986)

Table 3-4 Internal flow conditions at each trajectory point

Freestream Mach Number	Internal Flow Mach Number	Static Pressure, P (N/m^2)	Static Temperature T (K)	Density, ρ (kg/m^3)	Velocity Magnitude, V (m/s)	Specific Heat Ratio, γ	Gas Constant, R_g (J/kg/K)
10.0	2.0577	374453	2986.5	3.5232e-01	2373.7	1.2522	355.86
11.0	2.3700	318793	2993.4	2.9806e-01	2744.0	1.2534	357.31
12.0	2.6632	277896	3006.4	2.5752e-01	3099.3	1.2551	359.05
13.0	2.9437	245597	3022.5	2.2506e-01	3446.4	1.2562	361.03
14.0	3.2132	220519	3041.7	1.9957e-01	3787.8	1.2578	363.24
15.0	3.4746	199020	3062.2	1.7770e-01	4126.8	1.2596	365.71
16.0	3.7272	182149	3084.6	1.6028e-01	4462.9	1.2617	368.40
17.0	3.9736	167372	3107.3	1.4504e-01	4798.6	1.2639	371.32
18.0	4.2130	155104	3131.1	1.3228e-01	5133.6	1.2665	374.47
19.0	4.4474	144248	3154.5	1.2104e-01	5469.4	1.2692	377.80
20.0	4.6774	134601	3177.5	1.1109e-01	5806.2	1.2719	381.30
21.0	4.9037	126098	3199.8	1.0237e-01	6144.3	1.2748	384.93
22.0	5.1250	118488	3222.2	9.4597e-02	6483.8	1.2780	388.75
23.0	5.3435	111740	3243.5	8.7734e-02	6824.6	1.2809	392.62
24.0	5.5589	105282	3264.2	8.1311e-02	7168.0	1.2843	396.66
25.0	5.7666	100130	3284.8	7.6076e-02	7506.9	1.2877	400.70

3.3 External Flow

The external flow is an important variable in the analysis of the overall thrust of the nozzle because of its influence on the lower cowl and interaction with the interior flow through the location of the contact surface (refer to Figure 1-2). Since the vehicle shape and its influence on the external flow is unknown, an oblique shock solution was used to simply model the flow properties at the external cowl.

At hypersonic speeds, the temperature ratio across the shock (see Figure 3-3) is not modeled well with the thermally and calorically perfect gas. A thermally perfect, but calorically imperfect gas more accurately models the flow properties downstream of the oblique shock and was used to determine the external flow conditions. The procedure used was patterned after example 7-10 in Zucrow and Hoffman (1976).

The caloric model used was

$$h = \left(h_o + a\,T + \frac{b\,T^2}{2} + \frac{c\,T^3}{3} + \frac{d\,T^4}{4} + \frac{e\,T^5}{5} \right) R \qquad \textbf{(3-8)}$$

$$c_p = \left(a + b\,T + c\,T^2 + d\,T^3 + e\,T^4 \right) R \qquad \textbf{(3-9)}$$

where the coefficients (a, b, c, d, e) were obtained from curve fitted JANAF data (Gordon, 1989). With the thermally perfect gas, the mixture gas constant does not vary, allowing for easy calculation of the specific heat at constant volume with the following relation.

$$c_v = c_p - R \tag{3-10}$$

Therefore, the specific heat ratio is

$$\gamma = \frac{c_p}{c_v} \tag{3-11}$$

To determine the flow properties across the oblique shock, an initial deflection is needed. Using an angle of attack of two degrees and a forebody ramp of six degrees, the flow was turned a total angle of eight degrees. With the above gas model and the iterative shock solver, the external flow properties were determined and are summarized in Table 3-5. Again, representative values of specific heat ratio, $\gamma = 1.35$, and the mixture gas constant, R = 287 J/kg/K, were assumed to reduce the effects of multiple variables.

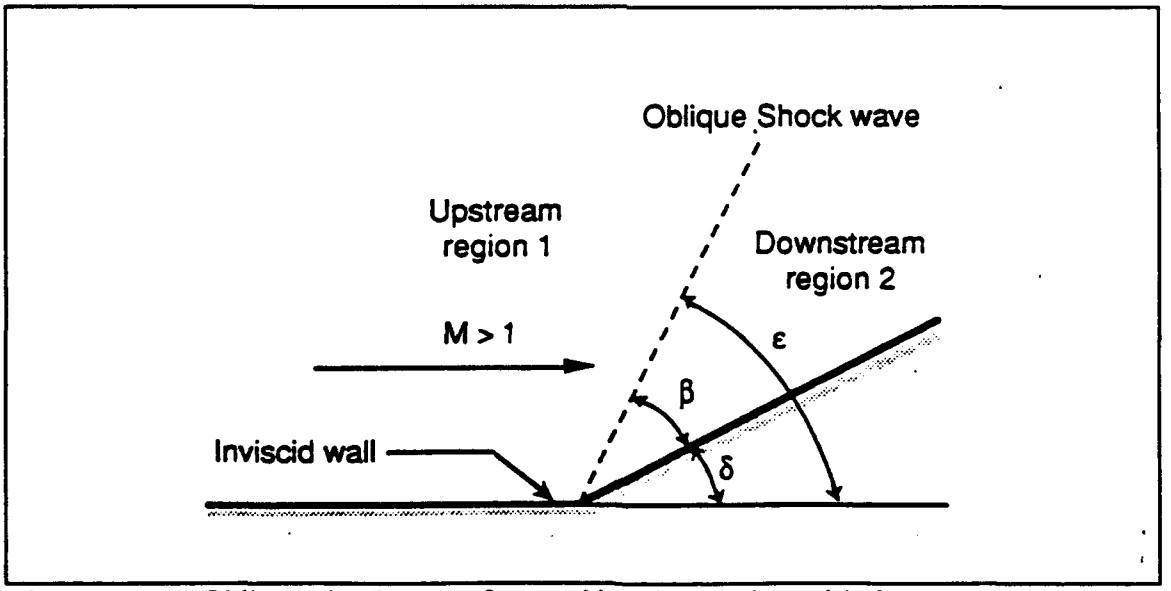

Figure 3-3 Oblique shock wave from vehicle interaction with free stream (Doty,1991:174)

Table 3-5 External flow conditions at each trajectory point

Freestream Mach Number	External Flow Mach Number	Shock Wave Angle, ε (deg)	Static Pressure, P (N/m^2)	Static Temperature T (K)	Density, ρ (kg/m^3)	Velocity Magnitude, V (m/s)	Specific Heat Ratio, γ	Gas Constant, R_g (J/kg/K)
10.0	7.311	12.360	3537.8	420.45	2.9308e-02	2998.9	1.3938	287.0
11.0	7.804	11.951	3332.0	455.35	2.5488e-02	3327.8	1.3909	287.0
12.0	8.261	11.622	3170.2	492.56	2.2418e-02	3659.2	1.3873	287.0
13.0	8.686	11.353	3032.5	532.23	1.9846e-02	3993.3	1.3833	287.0
14.0	9.081	11.130	2928.9	574.10	1.7770e-02	4329.0	1.3787	287.0
15.0	9.450	10.943	2831.6	618.45	1.5947e-02	4667.3	1.3737	287.0
16.0	9.796	10.783	2763.1	664.87	1.4476e-02	5006.6	1.3685	287.0
17.0	10.120	10.645	2699.2	713.62	1.3175e-02	5348.0	1.3630	287.0
18.0	10.426	10.525	2650.7	764.39	1.2078e-02	5690.5	1.3575	287.0
19.0	10.714	10.420	2606.2	817.41	1.1105e-02	6034.8	1.3520	287.0
20.0	10.986	10.326	2565.8	872.56	1.0242e-02	6380.8	1.3467	287.0
21.0	11.242	10.243	2529.9	929.83	9.4771e-03	6728.1	1.3417	287.0
22.0	11.485	10.168	2498.4	989.21	8.7973e-03	7076.8	1.3370	287.0
23.0	11.712	10.101	2471.4	1050.69	8.1933e-03	7426.6	1.3329	287.0
24.0	11.928	10.040	2439.7	1114.63	7.6240e-03	7778.8	1.3290	287.0
25.0	12.132	9.9851	2422.0	1179.21	7.1543e-03	8126.1	1.3253	287.0

IV Results and Discussion

4.1 Introduction

As stated in Chapter I, the purpose of this study was to determine the nozzle and cowl geometry combinations that produced maximum thrust for a hypersonic vehicle over a typical trajectory. In an effort to show the effects of the coupled optimization, the results were to be compared to an optimized nozzle without the coupled effect of a deflected cowl. This effort was successful.

This chapter discusses the results of the two parameter optimization and presents the results compared to a one parameter optimization of the nozzle contour. The nozzle attachment angle, θ_B and initial value data compiled in Chapter 3 were used in a one parameter optimization of the nozzle total thrust to obtain baseline data. The two parameter study used the nozzle attachment angle and a cowl deflection angle along with the same initial value data to optimize the total thrust of the configuration. The deflected cowl causes changes in the pressure field, affecting the forces on the nozzle and cowl walls; forces which can be optimized to produce the maximum thrust. The effects of a positive and negative cowl deflection were compared against the baseline for one point on the trajectory to motivate the purpose of this study. A comparison of the two optimizations was completed, showing the trends of the parameters and effects on the wall thrusts. A small study was also accomplished to motivate future study of varying the length of a deflected cowl .

4.2 Baseline - One Parameter Optimization

In order to analyse the results of the two parameter optimization, a baseline for comparison needed to be established. Previous work conducted by Herring (1991) optimized the nozzle contour (curve ABC in Figure 1-2) by using the nozzle attachment angle θ_B as the optimization parameter. That work was unsuited for this study for several reasons. First, he optimized the nozzle wall thrust whereas this study requires optimization of the total thrust; thrust contributions from the nozzle, upper cowl, and lower cowl walls. Herring (1991) also used a different scramjet cycle analysis code which produced a different internal initial value flow from the combustor exit (refer to Figure 1-2). Also, his study included only six points on the trajectory where this study established sixteen points. Therefore, this study includes a new one parameter optimization of the nozzle configuration, for a fixed cowl, over all trajectory points established in Section 3.

The results of optimizing the total thrust by changing the nozzle attachment angle are listed in Table 4-1. The table displays the nozzle attachment angle which produced the maximum total thrust of the nozzle/cowl configuration. The thrusts associated with the nozzle, upper and lower cowl walls are also presented for each trajectory point. The basic trend of the information in Table 4-1 indicates a decreasing total thrust as the trajectory is traversed and Mach number increases. The static pressure from the internal flow (Table 3-4) decreases with increasing Mach number along the trajectory. This decrease in pressure for the flow field results in a decrease in total wall thrust. With the decreasing static pressure, the nozzle attachment angle also decreases since the required

expansion to freestream pressure decreases. The upper cowl wall produces a small amount of thrust because of the small area projected in the axial direction (surface EF in Figure 1-2). Since the projected area is small, the thrust is two orders of magnitudes less then the thrust produced by the nozzle wall.

4.3 Cowl Deflection Effects

Since the nozzle attachment and cowl deflection angle are used in the two parameter optimization, the effects of the cowl deflection on the nozzle thrust is examined. The Mach 15 trajectory point was chosen as a representative case to illustrate the influence of the cowl deflection on the overall nozzle and cowl thrust performance. A positive and negative cowl deflection of 5 degrees were compared to the 0 degree baseline case obtained above.

To illustrate the effects of the deflected cowl, the flow field pressure patterns are discussed. Figure 4-1 represents the static pressure contours for the zero degree cowl deflection. Figure 4-2 and 4-3 represent the static pressure contours for the negative and positive cowl deflection, respectively. The figures show only one quarter of the flow field in order to provide adequate resolution of the features. The nozzle wall pressure distribution for the three cases is plotted in Figure 4-4 and discussed after the static pressure contours.

In Figure 4-1, expansion waves (1) stem from the nozzle opening to produce the rapid pressure drop in Figure 4-4. As the flow moves into the parabloic nozzle contour, the flow turns upon itself and a compression region (2) develops into a shock (3) structure

that curves away from the nozzle wall as the wave travels out of the nozzle. Above the shock (3), the flow begins to expand (4) along the nozzle wall even though the flow is still turning upon itself. This expansion (4) is caused by the cowl reflecting the initial expansion waves (5) which now dominate the flow. The reflected expansion waves (5) also affect the shock (3), causing the shock to curve and diminish. Another, smaller expansion (6) develops at the end of the cowl because of the cowl geometry.

In Figure 4-2, the greater second expansion (6) of the negative five degree cowl results in a lower pressure from the upper cowl wall to the shock (3) which tends to bring the shock (3) further from the nozzle wall. The pressure at the nozzle wall is now reduced resulting in reduced thrust. A shock wave (7) develops on the lower cowl, creating pressure drag and also reducing the total thrust.

In Figure 4-3, the positive five degree cowl causes a shock (8) to form from the cowl and is projected towards the nozzle wall. The shock (8) weakens the reflected expansion waves (5), causing a slightly higher pressure to be maintained aft of the shock (8). As the shock (8) reaches the nozzle wall, the higher pressure after the shock (8) can produce a greater pressure on the nozzle wall, thus creating higher thrust. The shock (8), along with the weakened reflected expansion (5), causes the curved shock (3) location to be closer to the nozzle wall than the zero cowl deflection case. With the curved shock (3) closer to the nozzle wall, a slight increase in pressure at the nozzle wall compared to the zero degree case is realized.

The higher pressure aft of the shock (8) also acts on the deflected cowl and can cause pressure drag, thereby reducing the total thrust of the nozzle/cowl configuration.

Table 4-2 shows the nozzle, upper, and lower cowl wall thrusts along with the total thrust for cowl deflection from -5 degrees to +5 degrees. The maximum total thrust occurs at the +1 deg cowl deflection. With greater positive deflection, the nozzle wall thrust continues to increase but the pressure drag on the upper cowl wall increases at a greater rate causing a net decrease in total thrust. Since the pressure of the external flow is low compared to the internal flow, the thrust produced by the lower cowl wall is very small compared to the nozzle wall thrust. With the negative cowl deflection, the upper cowl wall thrust increases but the nozzle wall thrust decreases more quickly to net a decreased total thrust. Thus, with a small positive cowl deflection, an increase in the pressure on the larger nozzle wall should produce more thrust without causing a large pressure drag on the smaller upper cowl wall.

To show the effect on thrust, the nozzle wall pressure distributions for the 0, -5, and +5 cowl deflections were plotted verses the height (y) of the nozzle. Figure 4-4, zero degree cowl deflection curve, shows the initial expansion (item (1) in Figure 4-1), by the sudden drop in pressure. As the flow moves into the parabolic nozzle contour (item (2) in Figure 4-1), a gradual pressure rise develops as the flow is turned upon itself. As the reflected expansion waves (item (5) in Figure 4-1), dominate the flow at the nozzle wall (item (4) in Figure 4-1), the pressure decreases as the nozzle expands the flow to the freestream pressure. With a negative 5 degree cowl deflection, the same initial drop and gradual rise in pressure develop since the inital nozzle/cowl geometry is the same. As the flow reaches the deflected cowl, a stronger expansion reduces the pressure throughout the remainder of the flow field which causes a reduced pressure at the nozzle wall. The

positive 5 degree cowl deflection begins the same as the other two; the initial geometry is the same. As the flow encounters the deflected cowl, a shock forms at the deflection and compresses the flow. The shock wave from the deflection impinges on the nozzle wall, giving the spike in the pressure curve, Figure 4-4. After the flow passes the compression, the expansion to freestream can take place. Since thrust for the planar geometry is based on pressure acting on an area by

$$\frac{Thrust}{w} = \int_{y_1}^{y_2} P \, dy \qquad (4\text{-}1)$$

the area under the curve in Figure 4-4 represents the above integral.

However, with the positive cowl deflection, there is pressure acting on the cowl's vertical area which results in a drag component. The balance of the nozzle wall thrust and the pressure drag on the deflected cowl wall motivates the two parameter optimization.

4.4 Two Parameter Optimization

With the baseline established and an understanding of how the cowl deflection should produce an increase in thrust, the next step is to perform the optimization. Following the procedure outlined in Section 2.5, the nozzle attachment angle and cowl deflection angle which maximized the total thrust were determined.

Since the magnitudes of the total thrust values vary from approximately 14700 N/m at Mach 10 to nearly 4600 N/m at Mach 25, a normalized thrust at each trajectory

point is calculated so comparison of two or more trajectory point data is more useful. The normalized thrust is calculated with the following expression:

$$(normalized\ thrust)_M = \frac{(thrust_{opt2})_M}{(thrust_{opt1})_M} \qquad (4\text{-}2)$$

The freestream Mach number is represented by M to identify the trajectory point, $(thrust_{opt2})_M$ is the two parameter optimized total thrust at Mach M, and $(thrust_{opt1})_M$ is the baseline one parameter optimized total thrust. With the above scaling, the baseline thrust normalizes to a value equal to 1. Any value from the two parameter optimization greater than 1 would indicate a thrust increase over the one parameter optimized total thrust.

Since all trajectory points have similar data trends, data from one point, Mach 15, is reviewed in detail. First, the total thrust data was normalized with the procedure explained above. Next, the normalized total thrust and the associated cowl deflection angle is plotted, in Figure 4-5, against the particular nozzle attachment angles. To provide a clear picture, only the data immediately surrounding the optimum data is displayed. All other thrust values are much less than one. Note the scale for the normalized thrust. All displayed thrust values are very near or above the normalized thrust over the range of nozzle attachment angles and varying cowl deflection angles. There is a range of nozzle attachment angles where the total thrust is at or above the normal total thrust value of 1. By deflecting the cowl, a nozzle wall designed for one Mach number can perform at an off design Mach number without significant loss of total thrust. The off design losses are beyond the scope of this study.

Another item of interest is the nozzle wall pressure plot, Figure 4-6. The baseline nozzle pressure is illustrated by the dashed line and the solid line is the pressure distribution of the two parameter optimized nozzle wall. Similar to Figure 4-1, the positive cowl deflection increased the nozzle wall pressure without excessive pressure drag on the cowl, thereby producing a greater total thrust over the baseline value.

With the maximum total thrust and corresponding nozzle attachment angle and cowl deflection angle determined from the two parameter optimization, an analysis of the parameters and total thrust over the trajectory was completed. In Table 4-3, the nozzle wall, upper cowl, lower cowl, and total thrust values with the associated nozzle attachment and cowl deflection angles are shown for each point on the trajectory.

A comparison of Table 4-1 and Table 4-3 shows the nozzle attachment angle from the two parameter optimization retains the same trend as the baseline data over the trajectory; the angle decreases as Mach number increases (see Figure 4-5) due to the decrease in static pressure at the nozzle entrance. The actual values of the angles differ only slightly at each trajectory point; the difference being due to the cowl deflection. The variable cowl deflection angle (Table 4-3) begins with a negative deflection at the lower Mach numbers, less than Mach 13, indicating the nozzle contour is insufficient to expand the flow to freestream pressure. As the cowl deflection turns positive and increases as the Mach number increases, the deflected cowl forms a shock wave which impinges on the nozzle wall, increasing the nozzle wall pressure. As the Mach number increases, the Mach angle decreases. For the shock wave from the deflected cowl to affect the nozzle wall pressure at increasingly high Mach numbers, the deflection must be increased to

overcome the decreasing Mach angle.

The nozzle wall thrust, Table 4-3, was increased with a positive cowl deflection, due to the pressure rise caused by the shock formed at the deflection increasing the nozzle wall pressure. The negative cowl delfection reduced the flow pressure by the expansion (5) of the flow illustrated in Figure 4-2. The flow field pressure also exerts a force on the upper and lower cowl surfaces, producing a thrust contribution, positive or negative. With the positive cowl deflection, the upper cowl wall (Figure 1-2) becomes a drag surface, reducing the total thrust of the nozzle/cowl configuration. The lower cowl wall is a propulsive surface with the positive cowl deflection. Since the external flow pressure is lower than the internal flow pressure, the resulting force on the lower cowl is quite small as seen in Table 4-3.

Table 4-4 displays the total thrust values from the one and two parameter optimizations. At the lower Mach numbers, the total thrust values for the two optimizations are similar. Some of the two parameter optimized total thrust values are even less than the one parameter optimized values, but through further analysis, explained below, these lower thrust values from the two parameter optimization were increased. These lower values were caused by the optimization procedure homing in on a plateau (refer to Figure 2-4) in the thrust curve. At the higher Mach numbers, and higher positive cowl deflection, the two parameter optimized thrust is greater than the one parameter optimized thrust.

The normalization process was applied to the total thrust values in Table 4-4. The results of this procedure are presented in Table 4-5 with a plot of the data, represented

by the solid line, in Figure 4-8. Recall any value greater than 1 represents an increase in total thrust for the two parameter optimization over the one parameter optimization. In Table 4-5, the normalized thrust for the Mach 13 and 14 cases are less than one, also indicated in Figure 4-8. In an effort to obtain greater thrust at all trajectory points, a third order curve fit for the two parameters, the nozzle attachment and cowl deflection angles, in Table 4-2 was accomplished using the Mach number as the independent variable. The dashed lines in Figure 4-7 represent the curve fit. Note the Mach 13 and 14 cases in Figure 4-7. The values of the two parameters do not lay on the curves. With the curve fit, new values of the two parameters were obtained and used as input to the FDS code to determine the associated thrusts. The new thrust values were compared to the values in Table 4-2 and nearly fifty percent were improved. The highest thrust with the associated parameters were retained and combined to form Table 4-6. Using the same normalization process as above, the total thrust data in Table 4-6 was normalized and the results were plotted as the dash line in Figure 4-8. With the curve fitted nozzle attachment and cowl deflection angles, the trend of the normalized total thrust over the trajectory was an increase in total thrust over the one parameter optimized total thrust at every point.

4.5 Cowl Length Effect on Thrust

Although not part of the original study, the length, xcwl2 in Figure 2-5, of a positively deflected cowl was briefly studied to give a better understanding of the cowl deflection effects. The Mach 20 trajectory point was chosen and only three lengths were

considered; the original length used in the optimization study, one shorter, and one longer. The nozzle attachment angle and cowl deflection angle used were obtained from the two parameter optimization study and were held constant for the three cases.

In Table 4-7, the nozzle wall, upper cowl and lower cowl wall thrusts for each deflected cowl length is displayed. With the short deflected cowl, the expansion (6), Figure 4-3, occurs closer to the nozzle entrance thereby reducing the flow pressure in the remainder of the nozzle compared to the thrust produced with the original length cowl. The upper cowl wall, with its reduced projected area, causes less pressure drag than the original length cowl. Even though there is less drag on the upper cowl wall, the loss of thrust producing pressure on the nozzle wall dominates, therefore the total thrust of the nozzle/cowl configuration with the shorter delfected cowl is less than the original total thrust.

The longer deflected cowl had the oposite effect on the nozzle wall thrust than the shorter deflected cowl. The additional length of the cowl cause the flow field pressure to be maintained further downstream by having the expansion (6), Figure 4-3, further downstream than the expansion of the original cowl. With the increased pressure in the flow field, the pressure at the nozzle wall is higher, thus creating greater thrust. Since the cowl length was greater than the original cowl length, the projected area of the deflected cowl was greater along with the associated pressure drag on the upper cowl surface, Table 4-7. The increased pressure drag on the lengthened cowl was dominated by the increased nozzle wall pressure, thus a net total thrust increase.

Table 4-1 Baseline thrust data - one parameter optimization

Mach Number	Nozzle Attach Angle (deg)	Cowl Angle Deflection (deg)	Nozzle Thrust (N/m)	Upper Cowl Thrust (N/m)	Lower Cowl Thrust (N/m)	Total Thrust (N/m)
10	35.987	0.00	-14650.07	-74.17	0.00	-14724.24
11	32.860	0.00	-13204.61	-74.74	0.00	-13279.35
12	29.751	0.00	-11966.80	-74.56	0.00	-12041.36
13	27.391	0.00	-10870.78	-73.75	0.00	-10944.53
14	25.590	0.00	-9954.38	-72.90	0.00	-10027.28
15	23.955	0.00	-9108.61	-71.42	0.00	-9180.03
16	22.641	0.00	-8414.36	-70.27	0.00	-8484.63
17	21.573	0.00	-7776.55	-68.84	0.00	-7845.39
18	20.021	0.00	-7226.97	-67.50	0.00	-7294.47
19	19.694	0.00	-6724.99	-66.06	0.00	-6791.05
20	18.755	0.00	-6266.27	-64.47	0.00	-6330.74
21	17.924	0.00	-5849.74	-63.08	0.00	-5912.82
22	17.575	0.00	-5469.62	-61.66	0.00	-5531.28
23	16.196	0.00	-5125.21	-60.32	0.00	-5185.53
24	16.092	0.00	-4792.91	-58.48	0.00	-4851.39
25	16.046	0.00	-4518.90	-57.22	0.00	-4576.12

Table 4-2 Thrust data - cowl deflection effects

Cowl Deflection	Nozzle Wall Thrust (N/m)	Upper Cowl Wall Thrust (N/m)	Lower Cowl Wall Thrust (N/m)	Total Thrust (N/m)
- 5 deg	-8554.252	-574.661	104.679	-9024.234
- 4 deg	-8640.900	-505.693	70.253	-9076.341
- 3 deg	-8738.267	-422.543	42.979	-9117.830
- 2 deg	-8848.015	-323.523	23.164	-9148.374
- 1 deg	-8970.539	-207.246	9.273	-9168.512
0 deg	-9108.608	-71.420	0.000	-9180.029
+ 1 deg	-9261.949	84.830	-6.253	-9183.372
+ 2 deg	-9432.037	263.424	-9.900	-9178.513
+ 3 deg	-9620.393	466.210	-11.818	-9166.001
+ 4 deg	-9832.633	696.937	-12.705	-9148.401
+ 5 deg	-10059.411	952.614	-12.487	-9119.284

Table 4-3 Thrust data - two parameter optimization

Mach Number	Nozzle Attach Angle (deg)	Cowl Angle Deflection (deg)	Nozzle Thrust (N/m)	Upper Cowl Thrust (N/m)	Lower Cowl Thrust (N/m)	Total Thrust (N/m)
10	36.185	-0.493	-14601.113	-130.005	5.098	-14726.020
11	33.391	-0.552	-13144.244	-140.471	5.452	-13279.264
12	30.277	-0.141	-11949.423	-92.601	1.233	-12040.79
13	29.358	0.007	-10864.727	-72.795	-0.057	-10937.580
14	25.409	1.640	-10201.166	185.541	-9.207	-10024.832
15	23.969	1.179	-9292.450	115.735	-7.072	-9183.788
16	21.638	0.971	-8570.934	87.610	-5.943	-8489.267
17	21.521	2.327	-8205.104	361.820	-10.017	-7853.301
18	19.924	2.289	-7667.522	368.746	-9.614	-7308.391
19	19.938	2.156	-7150.524	350.334	-9.163	-6809.354
20	18.447	2.362	-6750.217	406.062	-9.194	-6353.349
21	17.456	2.328	-6338.057	405.622	-8.460	-5940.894
22	17.586	2.759	-6074.464	518.821	-9.197	-5564.840
23	17.209	2.627	-5703.413	487.664	-8.990	-5224.738
24	16.200	3.131	-5514.860	623.474	-9.024	-4900.410
25	15.999	3.011	-5217.721	593.365	-8.899	-4633.255

Table 4-4 Total thrust comparison

Mach Number	Total Thrust (N/m) One Parameter Optimization	Total Thrust (N/m) Two Parameter Optimization
10	-14724.24	-14726.020
11	-13279.35	-13279.264
12	-12041.36	-12040.79
13	-10944.53	-10937.580
14	-10027.28	-10024.832
15	-9180.03	-9183.788
16	-8484.63	-8489.267
17	-7845.39	-7853.301
18	-7294.47	-7308.391
19	-6791.05	-6809.354
20	-6330.74	-6353.349
21	-5912.82	-5940.894
22	-5531.28	-5564.840
23	-5185.53	-5224.738
24	-4851.39	-4900.410
25	-4576.12	-4633.255

Table 4-5 Normalized thrust comparison

Mach Number	Normalized Total Thrust One Parameter Optimization	Normalized Total Thrust Two Parameter Optimization
10	1.0000	1.0001
11	1.0000	1.0000
12	1.0000	1.0000
13	1.0000	0.9994
14	1.0000	0.9998
15	1.0000	1.0004
16	1.0000	1.0005
17	1.0000	1.0010
18	1.0000	1.0019
19	1.0000	1.0027
20	1.0000	1.0036
21	1.0000	1.0047
22	1.0000	1.0061
23	1.0000	1.0076
24	1.0000	1.0101
25	1.0000	1.0125

Table 4-6 Thrust data - combined third order curve fit and two parameter optimized values

Mach Number	Nozzle Attach Angle (deg)	Cowl Angle Deflection (deg)	Nozzle Thrust (N/m)	Upper Cowl Thrust (N/m)	Lower Cowl Thrust (N/m)	Total Thrust (N/m)
10	36.185	-0.493	-14601.113	-130.005	5.098	-14726.020
11	33.273	-0.336	-13167.461	-115.303	3.194	-13279.570
12	30.277	-0.141	-11949.423	-92.601	1.233	-12040.79
13	28.023	0.508	-10938.236	-2.404	-3.761	-10944.402
14	25.908	0.877	-10080.363	58.325	-5.827	-10027.865
15	23.969	1.179	-9292.450	115.735	-7.072	-9183.788
16	22.548	1.514	-8665.243	183.900	-8.154	-8489.497
17	21.246	1.786	-8094.440	248.245	-8.760	-7854.955
18	19.924	2.289	-7667.522	368.746	-9.614	-7308.391
19	19.938	2.156	-7150.524	350.334	-9.163	-6809.354
20	18.447	2.362	-6750.217	406.062	-9.194	-6353.349
21	17.872	2.585	-6400.784	468.363	-9.256	-5941.677
22	17.586	2.759	-6074.464	518.821	-9.197	-5564.840
23	16.878	2.833	-5760.949	541.991	-9.089	-5228.047
24	16.200	3.131	-5514.860	623.474	-9.024	-4900.410
25	15.999	3.011	-5217.721	593.365	-8.899	-4633.255

Table 4-7 Cowl length effects on thrust - Mach 20

Deflected Cowl Length (m)	Nozzle Wall Thrust (N/m)	Upper Cowl Thrust (N/m)	Lower Cowl Thrust (N/m)	Total Thrust (N/m)
0.100	-6379.715	222.821	-6.146	-6163.039
0.154	-6750.217	406.062	-9.194	-6353.349
0.200	-6927.984	498.768	-11.875	-6441.091

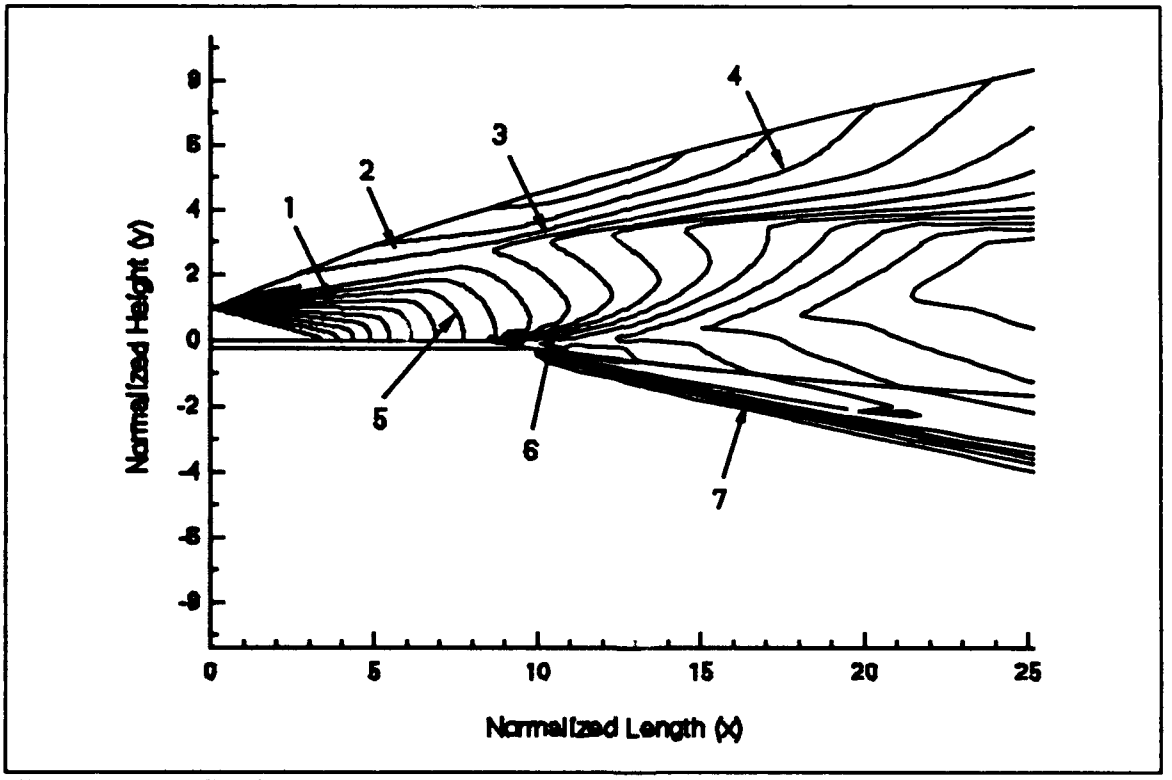

Figure 4-1 Static pressure contours, cowl deflection = 0 deg

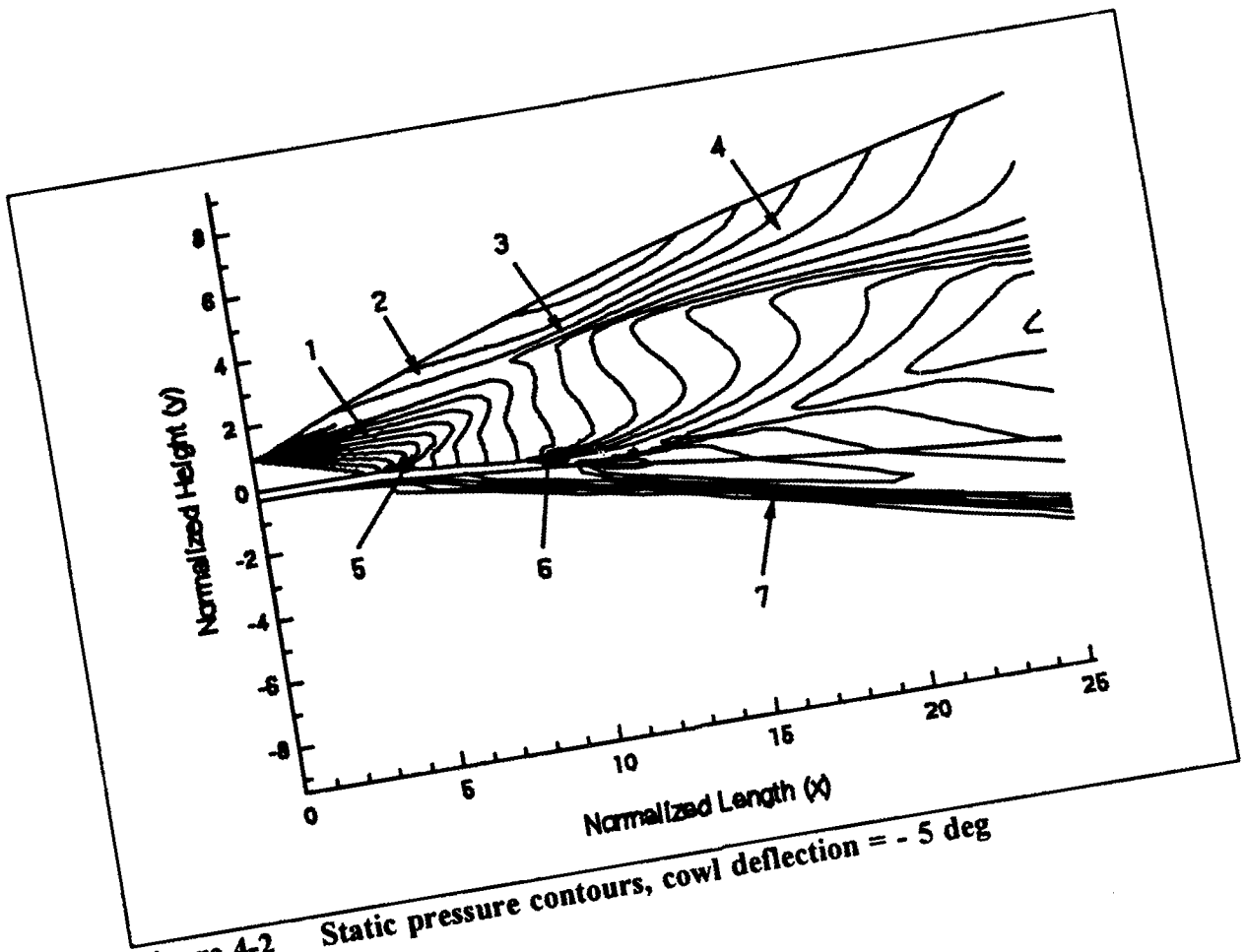

Figure 4-2 Static pressure contours, cowl deflection = - 5 deg

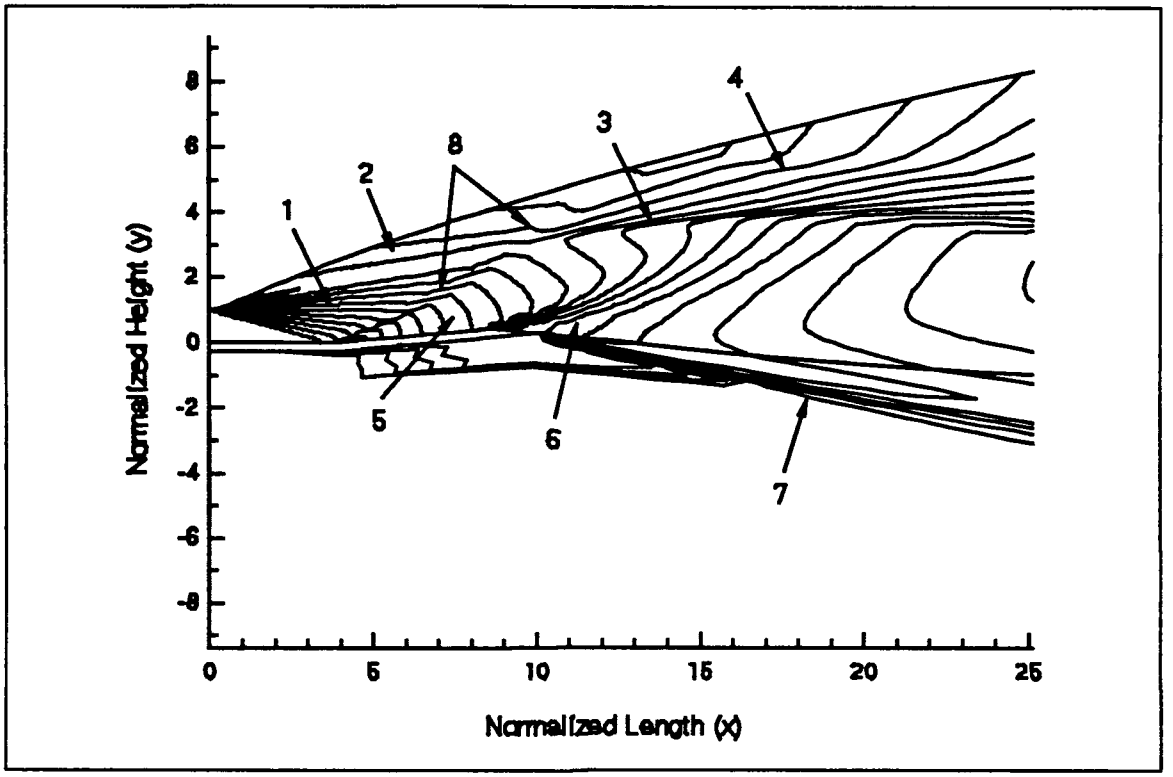

Figure 4-3 Static pressure contours, cowl deflection = + 5 deg

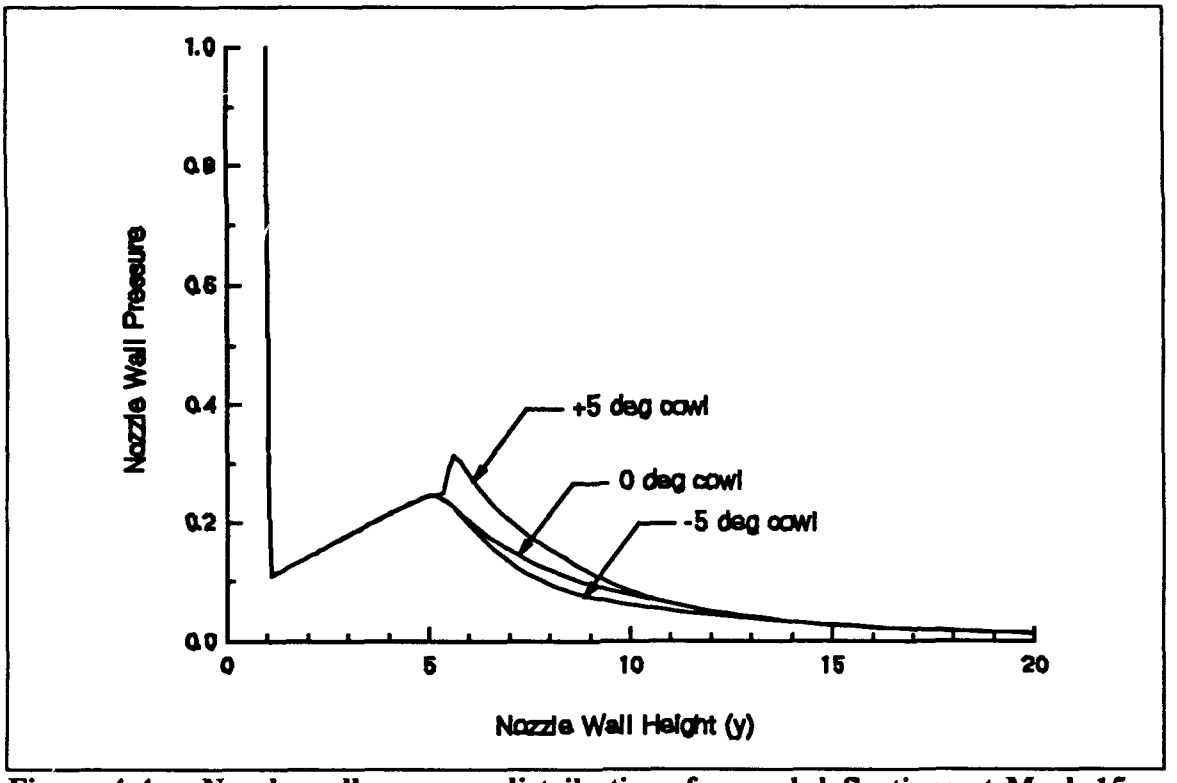

Figure 4-4 Nozzle wall pressure distributions for cowl deflections at Mach 15

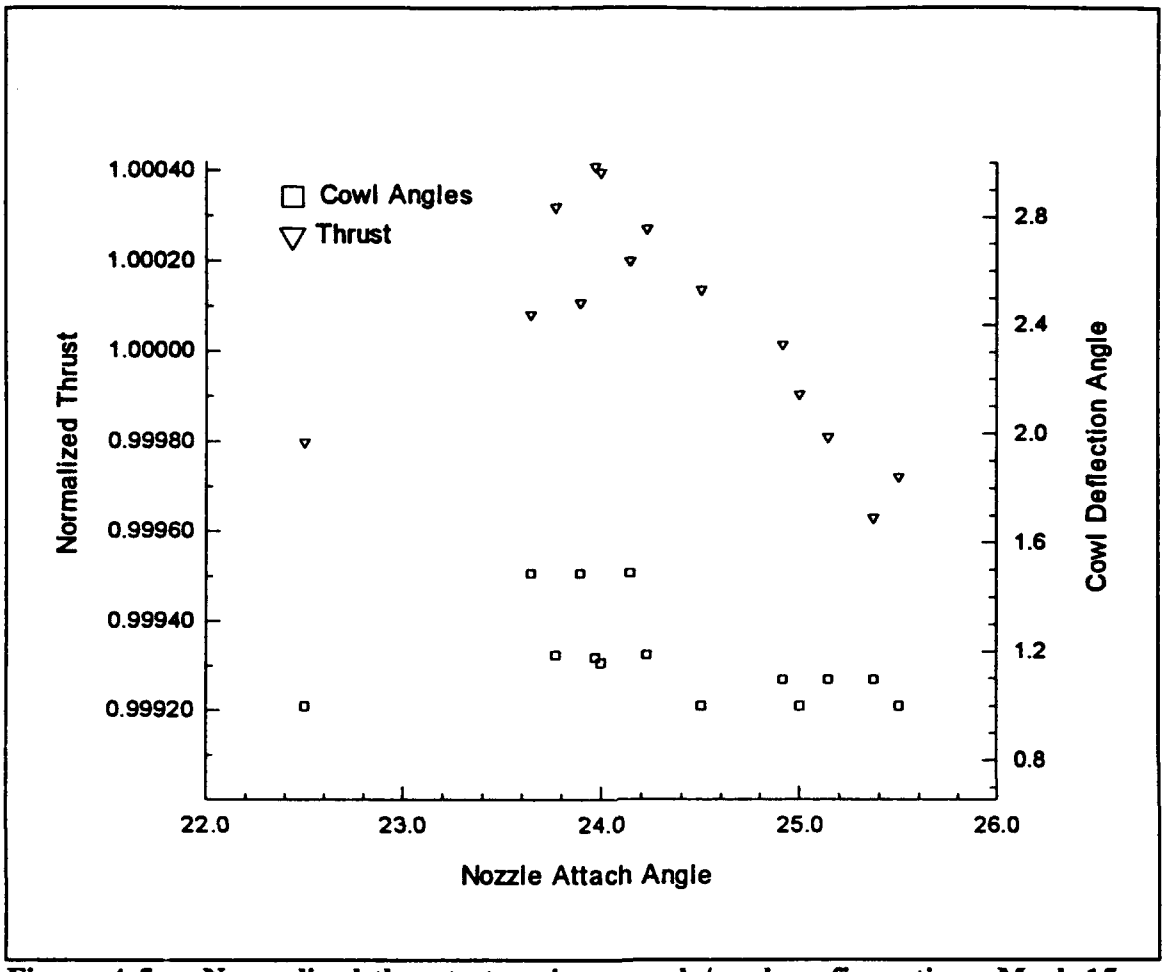

Figure 4-5 Normalized thrust at various nozzle/cowl configurations, Mach 15

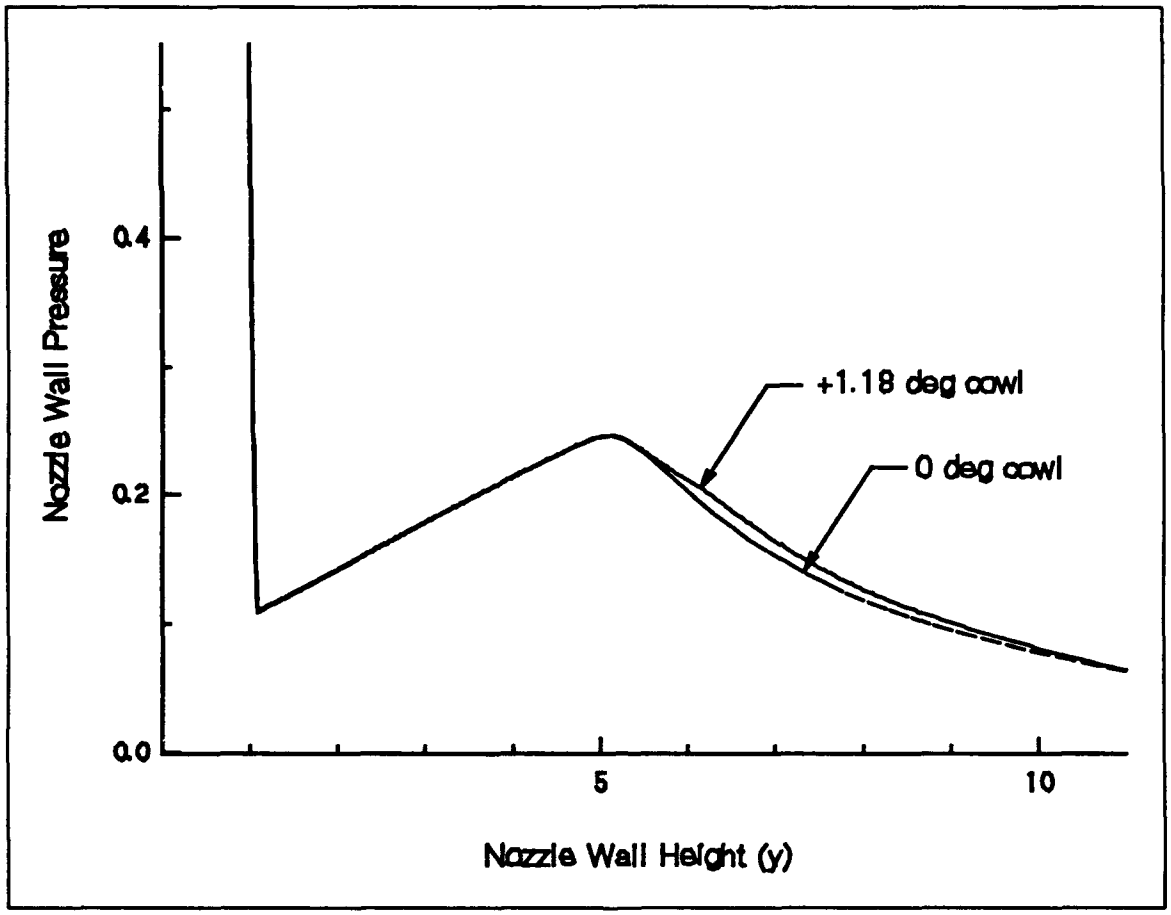

Figure 4-6 Nozzle wall pressure distribution for optimal nozzle/cowl

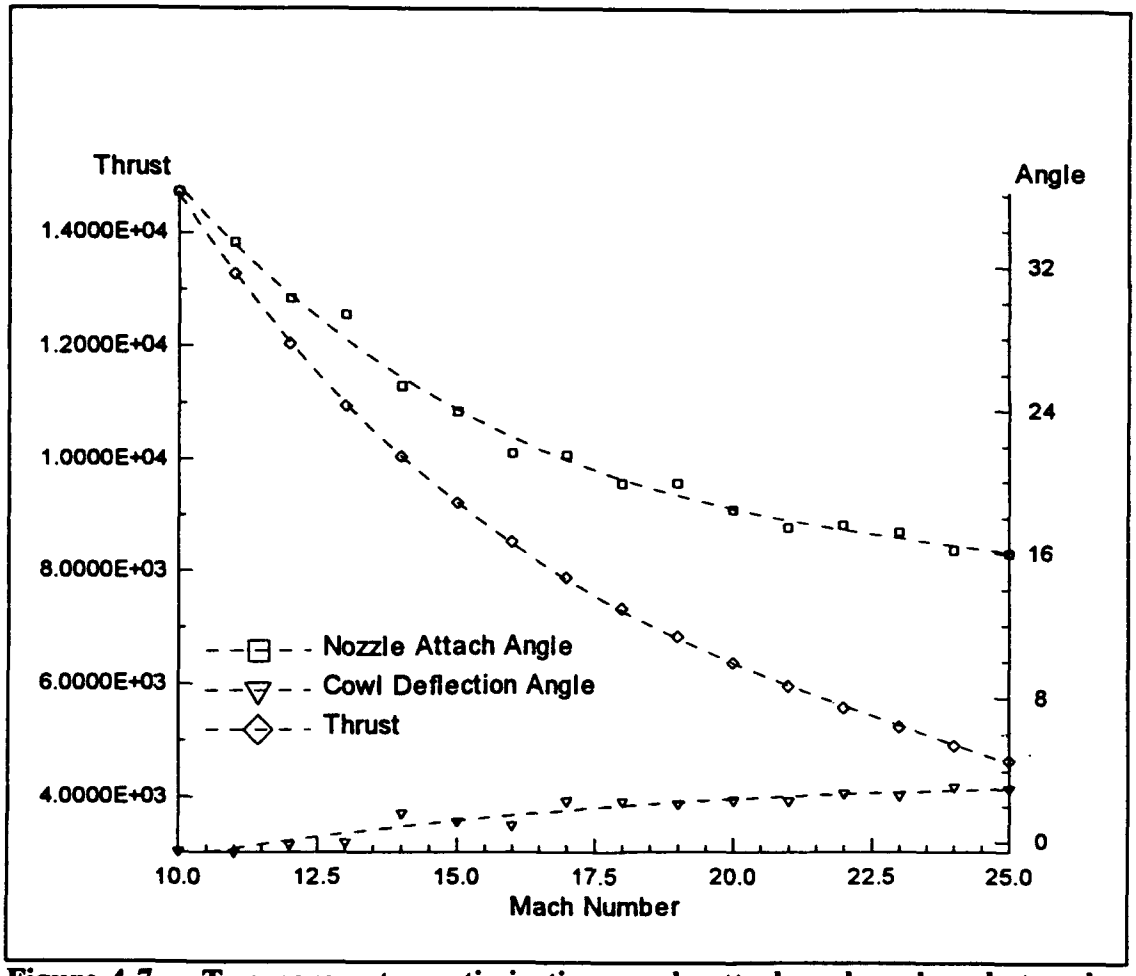

Figure 4-7 Two parameter optimization nozzle attach and cowl angle trends over the trajectory

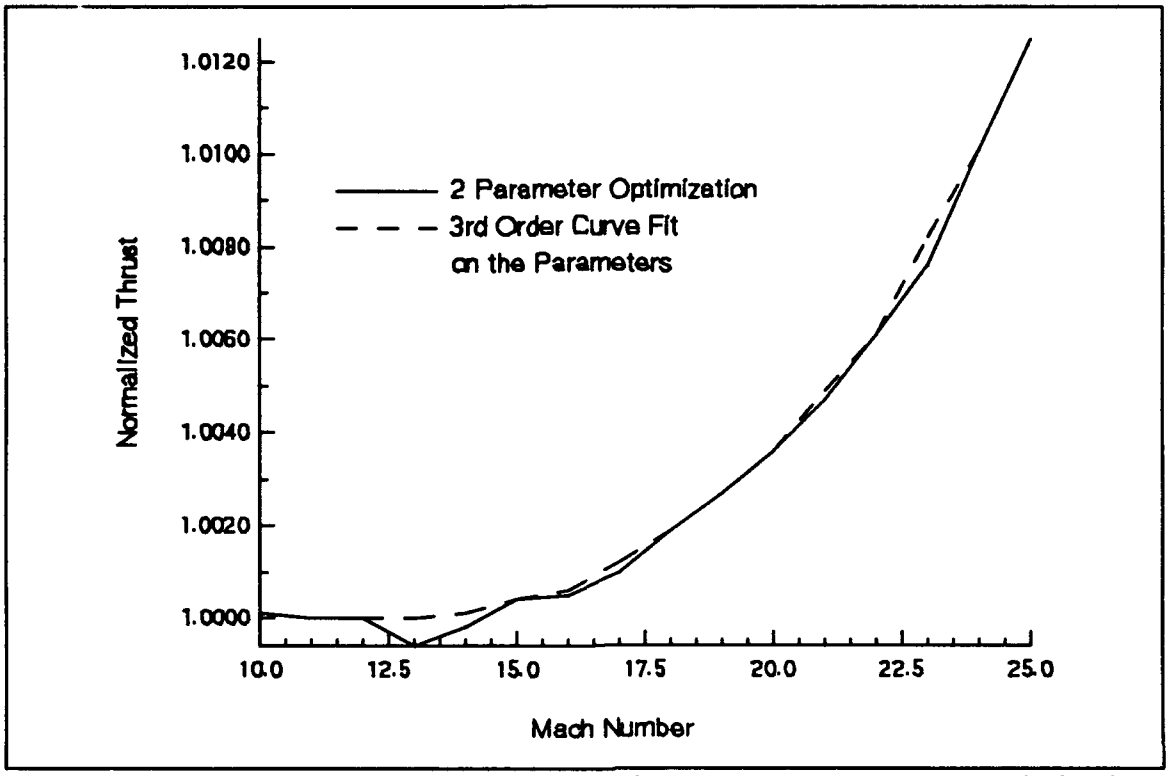

Figure 4-8 Normalized thrust over the trajectory - two parameter optimization

V Conclusions and Recommendations

5.1 Conclusions

This study has shown that a nozzle and cowl geometry combination can be optimized to produce maximum thrust performance for a hypersonic vehicle over a typical trajectory. The present study has also shown that a positively deflected cowl is the main cause of the thrust performance increase over an optimized nozzle with a straight cowl. Additionally, the thrust performance increase is greater at higher Mach numbers.

The trend of the optimal nozzle and cowl configuration producing maximum thrust was highly dependent upon the nozzle entrance pressure. The nozzle entrance pressure and Mach number were the driving factors for the amount of initial expansion along the circular arc which determined the nozzle attachment angle. The higher nozzle entrance pressure combined with the lower Mach number caused the greater nozzle attachment angle to expand the flow to free stream and vice versa.

The positively deflected cowl increased thrust performance by forming a pressure rise in the nozzle flow field by the formation of a shock wave. The trade-off of increased thrust on the nozzle wall and pressure drag on the upper cowl wall produced an increase in total thrust for the nozzle/cowl configuration over the straight cowl configuration.

As the Mach number increases, the thrust performance of the two parameter optimized nozzle/cowl configuration over the one parameter optimized nozzle increased. With increasing Mach numbers, the Mach angle decreases, causing the influence of the reflected expansion waves to move toward the aft portion of the nozzle wall. The area

of the nozzle wall from the shock wave impingement point to the reflected expansion wave impingement point increases with decreasing Mach angle. This increased area causes the increased thrust performance of the two parameter optimized nozzle/cowl configuration over the one parameter optimized nozzle.

5.2 Recommendations for Further Study

The data contained in this study are useful for trend analysis only since several simplifications were made such as the vehicle geometry, the use of a one-dimensional ramjet cycle program (since actual experimental data is scarce), and variable geometry nozzle and cowl which exceeds mechanical systems in variation tolerance. With this in mind, other trend analysis is needed to supplement the current work.

1. Optimization of the Cowl Deflection Angle and Length.

In the current study the length of the deflected cowl was varied for the purpose of determining the effects of the deflected cowl on the flow field. In the investigation, greater total thrust was produced by lengthening the deflected cowl. Although the thrust was increased, the pitching moment of the nozzle also changed. To fully determine the effect of the deflected cowl length, it is recommended that a two parameter optimization using the cowl deflection angle and length be conducted maximizing total thrust along with a limitation on pitching moment.

2. Optimization of the Cowl Deflection Angle and Position from the Nozzle Entrance.

Since the deflected cowl has pressure forces acting on it, a structural load limit

will apply to the cowl. With this load limit, the length of the deflected cowl is subject to a limit. The position of the deflected cowl from the nozzle entrance could give a greater range of variable geometry over the fixed position, variable length deflected cowl. Therefore, it is recommended that a two parameter optimization with the cowl deflection position and angle for a fixed nozzle contour be undertaken to maximize total thrust while limiting the cowl wall forces.

Bibliography

Billig, Frederick S. and Van Wie, David M. "Efficiency Parameters for Inlets Operating at Hypersonic Speeds,"Journal of the American Institute of Aeronautics and Astronautics, ISABE 87-7047 XX: 118-130 (1987).

----. "Combustor Inlet Interaction in Scramjet Engines,"AFL Technical Review, 2:1: 118-126 (1990).

Doty, John H. Maximum Thrust Planar Supersonic Nozzles Using a Flux-Difference-Splitting Technique. Ph.D Dissertation. School of Engineering, Purdue University, West Lafayette IN, August 1991.

Godunov, S. K., (1959), "A Finite-Difference Method for the Numerical Computation of Discontinuous Solutions of the Equations of Fluid Dynamics," Matematiceskii Sbornik, 47: 271-290 (1959) also Cornell Aeronautical Laboratory translation.

Gordon, Sanford and Bonnie J. McBride. Computer Program for Calculation of Complex Chemical Equilibrium Compositions, Rocket Performance, Incident and Reflected Shocks, and Chapman-Jouguet Detonations. NASA Special Publication SP-273. NASA Lewis Research Center, Interim Revision, March 1976, CET89 Update, 1989.

Henry, John R. and Anderson, Griffin Y. Design Considerations for the Airframe-Integrated Scramjet. NASA Technical Memorandum X-2895. Washington: NASA Science and Technical Information Office, 1973.

Herring, David J. Design of an Optimum Thrust Nozzle for a Typical Hypersonic Trajectory Through Computational Analysis. Masters Thesis. School of Engineering, Air Force Institute of Technology, Wright-Patterson AFB, OH, December 1991.

Kerrebrock, Jack L. Aircraft Engines and Gas Turbines. Cambridge MA: The MIT Press, 1981.

Mack, J. T., Stroh, C. W., Kozacka, J. D. Hypersonic Aircraft Propulsion Installation. Report for Wright Laboratory, Flight Dynamics Directorate, Air Force Systems Command, Wright-Patterson AFB, OH, January 1991 (WL-TR-91-3031).

Osher, S., (1981), "Numerical Solution of Singular Perturbation Problems and Hyperbolic Systems of Conservation Laws," Analytical and Numerical Approaches to Asymptotic Problems in Analysis, North Holland Mathematical Studies No. 47, Edited by S. Axelsson, L. S. Frank, and A. van der Sluis, 179-205, 1981.

Pandolfi, M. "Computation of Steady Supersonic Flows by a Flux-Difference-Splitting Method," Computers and Fluids, 10:1: 37-46 (1985).

Pandolfini, P. Instructions for Using RAMJET Performance Analysis (RJPA) - IBM-PC Version 1.0. Contract JHU/APL-NASP-86-2. Laurel MD: The John Hopkins University Applied Physics Laboratory, November, 1986.

Peyret, R. and Taylor, T. D. Computational Methods for Fluid Flow. New York: Springer-Verlag Corp, 112-115 (1983).

Taylor, T. D., Ndefo, E., Masson, B. S. "A Study of Numerical Methods for Solving Viscous and Inviscid Flow Problems," Journal of Computational Physics, 9:5: 99-119 (1972).

United States Committee on Extension to the Standard Atmosphere. US Standard Atmosphere, 1976. Washington: Government Printing Office, October 1976.

Walton, James T. An Overview of Airframe Integrated Scramjet Cycle Components and Flow Features. NASP Technical Memorandum 1029. Langley VA: NASA Langley Research Center, November 1988.

Zucrow, Maurice J. and Joe D. Hoffman. Gas Dynamics, Volume I. New York: John Wiley and Sons, Inc., 1976.

Vita

Michael J. Bonaparte was born on 28 July 1961 in Greenville, South Carolina. He was graduated from Brother Rice High School in Chicago, Illinois in 1979. From there he went on to attend Parks College of Saint Louis University in Cahokia, Illinois where he received the degree of Bachelor of Science in Aerospace Engineering in July 1982. After graduation, Mr Bonaparte joined the Air Force and received a commission through the Officer Training School, and was assigned to the San Antonio Air Logistics Center at Kelly AFB, Texas. While there, he worked in the Item Management Division as a project engineer on the Advanced Concept Ejection Seat and structural components of the C-5A engine pylons, cowls and thrust reversers. In 1988, then Captain Bonaparte was selected to serve as the Chief of the Advertising and Promotion Branch, 3552 USAF Recruiting Squadron at Wright-Patterson AFB, Ohio. He continued his duties there until May 1991, when he was accepted into the Air Force Institute of Technology's graduate engineering program in Aeronautical Engineering.

REPORT DOCUMENTATION PAGE

Form Approved
OMB No. 0704-0188

1. AGENCY USE ONLY *(Leave blank)*	2. REPORT DATE	3. REPORT TYPE AND DATES COVERED
	December 1992	Masters Thesis

4. TITLE AND SUBTITLE

Nozzle/Cowl Optimization for a Hypersonic Vehicle on a Typical Trajectory

5. FUNDING NUMBERS

6. AUTHOR(S)

Michael J. Bonaparte

7. PERFORMING ORGANIZATION NAME(S) AND ADDRESS(ES)

Air Force Institute of Technology
Wright-Patterson AFB, Ohio

8. PERFORMING ORGANIZATION REPORT NUMBER

AFIT/GAE/ENY/92D-10

9. SPONSORING / MONITORING AGENCY NAME(S) AND ADDRESS(ES)

10. SPONSORING / MONITORING AGENCY REPORT NUMBER

11. SUPPLEMENTARY NOTES

12a. DISTRIBUTION / AVAILABILITY STATEMENT

Unlimited Distribution

12b. DISTRIBUTION CODE

13. ABSTRACT *(Maximum 200 words)*

An investigation of the effects of simultaneous variation of the nozzle attachment and cowl deflection angle on the performance of a two-dimensional nozzle used on a hypersonic vehicle such as the National Aero-Space Plane (NASP) was performed using a two parameter optimization procedure. Total thrust optimization was accomplished using a Flux-Difference-Split (FDS) code, a RAMJET Performance Analysis program, and an oblique shock wave solver program, at sixteen points on a 1000 psf dynamic pressure trajectory for Mach numbers from 10.0 to 25.0. A single parameter optimization of the total thrust using a variable nozzle attachment angle was accomplished first to establish a reference frame. Effects of a deflected cowl on the nozzle flow field were explored. The optimum nozzle attachment and cowl deflection angle maximized the total thrust by increasing nozzle wall pressure without an excessive increase in pressure drag. The total thrust found by the two parameter optimization was increased at every point on the trajectory over the total thrust obtained from the single parameter optimization. This study shows that the cowl deflection angle starts negative, increasing from -0.493 degrees at Mach 10 to 3.01 degrees at Mach 25.

14. SUBJECT TERMS	15. NUMBER OF PAGES
Hypersonic Nozzle, Optimum Thrust Nozzle, Scramjet Nozzle Optimization, Hypersonic Vehicle	80
	16. PRICE CODE

17. SECURITY CLASSIFICATION OF REPORT	18. SECURITY CLASSIFICATION OF THIS PAGE	19. SECURITY CLASSIFICATION OF ABSTRACT	20. LIMITATION OF ABSTRACT
UNCLASSIFIED	UNCLASSIFIED	UNCLASSIFIED	UL